

# Functions of the Persistent Na<sup>+</sup> Current in Cortical Neurons Revealed by Dynamic Clamp

J.F. Storm, K. Vervaeke, H. Hu, and L.J. Graham

**Abstract** Many cortical neurons and other vertebrate nerve cells are equipped with a persistent Na<sup>+</sup> current,  $I_{\text{NaP}}$ , which operates at membrane potentials near the action potential threshold. This current may strongly influence integration and transduction of synaptic input into spike patterns. However, due to the lack of pharmacological tools for selective blockade or enhancement of  $I_{\text{NaP}}$ , its impact on spike generation has remained enigmatic. By using dynamic clamp to cancel or add  $I_{\text{NaP}}$  during intracellular recordings in rat hippocampal pyramidal cells, we were able to circumvent this long-standing problem. Combined with computational modeling our dynamic-clamp experiments disclosed how  $I_{\text{NaP}}$  strongly affects the transduction of excitatory current into action potentials in these neurons. First, we used computational model simulations to predict functional roles of  $I_{\text{NaP}}$ , including unexpected effects on spike timing and current–frequency relations. We then used the dynamic-clamp technique to experimentally test and confirm our model predictions.

## 1 Introduction

The integration and transduction of synaptic input to patterns of action potentials involve a delicate and complex interplay between membrane currents operating at potentials near the spike threshold, and the larger currents underlying the action potential. The former, the “subthreshold currents” or “threshold currents” are often pivotal for determining spike pattern, timing, and frequency. Among the most enigmatic of the subthreshold currents operating in mammalian neurons is the persistent sodium current ( $I_{\text{NaP}}$ ) (Crill, 1996). This current is likely to play important roles in mammalian cortical neurons, including synaptic integration and spike firing, as well as subthreshold oscillations and network

---

J.F. Storm (✉)

Department of Physiology at Institute of Basal Medicine, and Centre of Molecular Biology and Neuroscience, University of Oslo, pb 1103 Blindern, N-0317 Oslo, Norway  
e-mail: j.f.storm@medisin.uio.no

rhythmicity, e.g., in the hippocampus, entorhinal cortex (EC), neocortex (Alonso & Llinas, 1989; French & Gage, 1985), and subcortical and cerebellar neurons (Llinas & Sugimori, 1980; Llinas, 1988; Taddese & Bean, 2002).

However, it has been particularly difficult to test the functional roles of  $I_{\text{NaP}}$  in firing behavior because it has proved virtually impossible to selectively manipulate this current with specific pharmacological tools. A likely reason for these difficulties is that  $I_{\text{NaP}}$  appears to arise from the same channel population that underlies the classical spike-generating transient  $\text{Na}^+$  current ( $I_{\text{NaT}}$ ). Thus, different states or gating modes of the same  $\text{Na}^+$  channels may generate both  $I_{\text{NaP}}$  and  $I_{\text{NaT}}$  (Alzheimer et al., 1993; Crill, 1996; Taddese & Bean, 2002). Therefore, while functions of many other ionic currents have been determined by using specific pharmacological blockers and openers, or genetic manipulations, such approaches are problematic for  $I_{\text{NaP}}$  since manipulations that suppress this current will often suppress the spike-generating transient current, thus blocking firing and obscuring specific effects of  $I_{\text{NaP}}$ . In particular, blockers of  $I_{\text{NaP}}$  such as tetrodotoxin (TTX), riluzole, or phenytoin also directly affect  $I_{\text{NaT}}$ , reducing the amplitude of action potentials or eliminating them all together. Reduction of spike amplitude will in turn change the activation of voltage- and calcium-gated ion channels that mediate feedback regulation of spike frequency and spike pattern, thus distorting the effects of  $I_{\text{NaP}}$  (see below).

To circumvent these problems, we used dynamic clamp (Fig. 1) to study  $I_{\text{NaP}}$  both by the selective subtraction of this current (i.e. canceling out the native

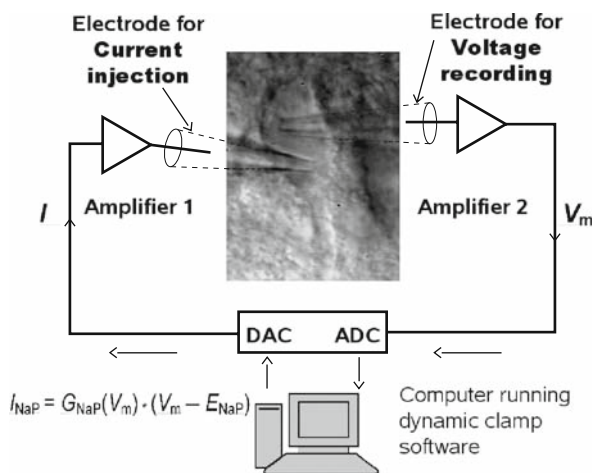


**Fig. 1 Dynamic-clamp configuration for analysis of  $I_{\text{NaP}}$  functions in hippocampal pyramidal neurons.** Diagram of the dynamic-clamp configuration, with two patch pipettes in whole-cell configuration at the soma of a CA1 pyramidal cell in a rat hippocampal slice: one pipette for voltage recording (*right*), the other for current injection (*left*).  $I_{\text{NaP}}$  it was calculated by the dynamic-clamp software, based on our  $I_{\text{NaP}}$  model and the measured membrane potential. To add the simulated  $I_{\text{NaP}}$ , the calculated current was injected into the cell in real time. To cancel the intrinsic  $I_{\text{NaP}}$  generated by the cell, a negative current equal to the simulated  $I_{\text{NaP}}$  was injected into the cell. (Modified from Vervaeke et al., 2006, with permission from *Cell Press, Elsevier*.)

current), as well as by the addition of a simulated  $I_{\text{NaP}}$  after the native  $I_{\text{NaP}}$  had been pharmacologically blocked. These tests were combined with other electrophysiological measurements from CA1 pyramidal neurons in hippocampal slices, and with simulations with a biophysically detailed compartmental model of this neuronal type.

## 2 Persistent Na<sup>+</sup> Current: History, Properties, and Functions

Many mammalian neurons show a noninactivating, TTX-sensitive sodium current component that begins to activate several millivolts negative to the spike threshold (Crill, 1996). The Hodgkin & Huxley (1952) (HH) equations for the fast inactivating Na<sup>+</sup> current ( $I_{\text{NaT}}$ ) underlying action potentials imply that this conductance also gives rise to a noninactivating current component at a limited range of membrane potentials due to the overlap between the activation and inactivation curves – a “window current” (see below, Fig. 5). Many neurons, however, show a distinct persistent Na<sup>+</sup> current,  $I_{\text{NaP}}$ , which is active far beyond the expected range of the classical HH window current and is thus apparently due to another mechanism (French & Gage, 1985; Crill, 1996). There is now good evidence that such an  $I_{\text{NaP}}$  can be caused wholly or partly by the same channel population as  $I_{\text{NaT}}$ , due to incomplete inactivation of these channels, or through some forms of modal gating (Aldrich et al., 1983; Alzheimer et al., 1993; Taddese & Bean, 2002). In addition, there is evidence that  $I_{\text{NaP}}$  may be caused partly by Na<sup>+</sup> channels that are biophysically and/or molecularly distinct from those underlying  $I_{\text{NaT}}$ , perhaps due to different subunit composition or modulation (Magistretti & Alonso, 1999; Magistretti & Alonso, 2002). Different mixtures of these mechanisms may contribute to various degrees in different cell types (Crill, 1996; Taddese & Bean, 2002).

Chandler & Meves (1966) found that the Na<sup>+</sup> current in squid axon shows incomplete inactivation, and Gilly & Armstrong (1984) identified a distinct population of Na<sup>+</sup> channels selectively activated by small depolarizations. However, the existence of a persistent Na<sup>+</sup> current in the brain was first inferred from intracellular current-clamp recordings from hippocampal and neocortical pyramidal neurons (Hotson et al., 1979; Connors et al., 1982) and cerebellar Purkinje cells (Llinas & Sugimori, 1980), revealing an increase in slope resistance – an “anomalous rectification” – starting ~10 mV negative to the spike threshold, apparently due to a noninactivating Na<sup>+</sup> current. Voltage-clamp measurements of such a current were first performed in cardiac Purkinje fibers (Attwell et al., 1979) and neocortical pyramidal neurons (Stafstrom et al., 1982). Subsequently,  $I_{\text{NaP}}$  has been studied in numerous neuronal types (Crill, 1996).

$I_{\text{NaP}}$  typically turns on upon membrane depolarization positive to ~-65 mV, activates and deactivates fast (within ~5 ms), and shows either no or very slow inactivation (time constant ~2–6 s) (French et al., 1990; Magistretti & Alonso, 1999). It has for long been debated whether this current has a separate molecular identity from  $I_{\text{NaT}}$ . However, converging evidence now seems to support

the conclusion that  $I_{\text{NaP}}$  is caused by a separate, noninactivating or slowly inactivating gating mode and/or incomplete inactivation of the  $I_{\text{NaT}}$  channels, in pyramidal cells and at least some other neurons (Alzheimer et al., 1993; Taddese & Bean, 2002).

$I_{\text{NaP}}$  has been shown to enhance both excitatory and inhibitory postsynaptic potentials (EPSPs and IPSPs) in neocortical (Stafstrom et al., 1985; Stuart & Sakmann, 1995; Stuart, 1999) and hippocampal pyramidal neurons (Lipowsky et al., 1996; Vervaeke et al., 2006). Furthermore, there is evidence that  $I_{\text{NaP}}$  amplifies the after-depolarization following a spike and can change the firing mode of CA1 pyramidal neurons from solitary spikes to spike bursts (Jensen et al., 1996; Yue et al., 2005). In addition,  $I_{\text{NaP}}$  drives spontaneous rhythmic firing in tuberomammillary neurons (Taddese & Bean, 2002).

In CA1 hippocampal pyramidal cells, we have shown that  $I_{\text{NaP}}$  engages in interesting interactions with the M-current (Kv7/KCNQ current), a persistent potassium current that is active in the subthreshold voltage range (Brown & Adams, 1980). Thus we found that  $I_{\text{NaP}}$  amplifies a form of subthreshold intrinsic neuronal resonance at theta frequencies ( $\sim 8$  Hz) that is mediated by M-current (called *M-resonance*) (Hu et al., 2002). In a later study we also showed how  $I_{\text{NaP}}$  amplifies after-hyperpolarizations (AHPs), how it affects the relation between injected depolarizing current ( $I$ ) and the resulting discharge frequency ( $f/I$  relation), and how it has contrasting effects on spike timing in CA1 pyramidal neurons (Vervaeke et al., 2006).

### 3 Why Use Dynamic Clamp to Study $I_{\text{NaP}}$ ?

#### 3.1 Lack of Specific Blockers of $I_{\text{NaP}}$

We used dynamic clamp for studying  $I_{\text{NaP}}$  functions in order to overcome the lack of specific pharmacological blockers. While some influential studies have used a low dose of TTX ( $\sim 5$  nM) to study  $I_{\text{NaP}}$  with only small effects on the spike shape (Jensen et al., 1996; Stuart, 1999), this approach is generally not suitable for studying the input–output relations in neurons, including repetitive firing and current-to-frequency transduction, since subtle changes in the spike shape can nevertheless have large consequences for these properties. Thus, a slight reduction in spike amplitude could strongly reduce the activation of voltage- and  $\text{Ca}^{2+}$ -dependent  $\text{K}^+$  channels underlying the AHPs, which are among the main determinants of the input–output relations of a neuron (Madison & Nicoll, 1984; Peters et al., 2005; Vervaeke et al., 2006; Gu et al., 2007).

A drug that has been used as a more selective blocker of  $I_{\text{NaP}}$  is the neuroprotective agent riluzole (Urbani & Belluzzi, 2000). However, at higher concentrations riluzole can also block  $I_{\text{NaT}}$  in the inactivated state (Benoit & Escande, 1991) and also block various axonal  $\text{K}^+$  currents (Benoit & Escande, 1993). However, the concentration necessary to substantially block  $I_{\text{NaP}}$  was

also found to affect the  $I_{\text{NaT}}$  amplitude (Urbani & Belluzzi, 2000). Moreover, riluzole has also potent effects on two-pore domain (2P) potassium channels (TREK-1 and TRAAK) (Duprat et al., 2000), which are major contributors to the resting K<sup>+</sup> leak current and thus important determinants of neuronal excitability throughout the central nervous system (Goldstein et al., 2001). Riluzole has also been reported to block high-voltage-activated Ca<sup>2+</sup> channels at concentrations used to block  $I_{\text{NaP}}$  (Huang et al., 1997). Thus, although it has often been used for blocking  $I_{\text{NaP}}$ , riluzole is not selective.

The anti-epileptic drug phenytoin (Mattson et al., 1985) has also often been used as a blocker  $I_{\text{NaP}}$  (Chao & Alzheimer, 1995). It seems that phenytoin stabilizes  $I_{\text{NaT}}$  in the inactivated state at similar concentrations that blocks  $I_{\text{NaP}}$ , thus having an activity-dependent effect on  $I_{\text{NaT}}$  (Kuo & Bean, 1994). Fricker & Miles (2000) found that phenytoin dramatically reduced the amplitude of the later spikes during repetitive firing in CA1 pyramidal neurons, although it had little effect on the first spike. Phenytoin has also been reported to block high-voltage-gated Ca<sup>2+</sup> channels at concentrations relevant for blocking  $I_{\text{NaP}}$  (Jeub et al., 2002). Thus, this blocker also seems unsuitable for studying the role of  $I_{\text{NaP}}$  in input–output relations of neurons.

### 3.2 *Perisomatic Localization of $I_{\text{NaP}}$ in Cortical Pyramidal Neurons*

A major limitation of dynamic clamp is that it can fully cancel or mimic conductances only if they arise at the subcellular localization where the patch pipette(s) contact(s) the cell. Because the exact molecular identity of  $I_{\text{NaP}}$  channels is uncertain, their distribution has not been determined by immunohistochemistry. Nevertheless, converging evidence suggests that  $I_{\text{NaP}}$  in cortical pyramidal neurons originates near the soma, probably at the axon initial segment (Stuart & Sakmann, 1995; Astman et al., 2006). An elegant study by Stuart & Sakmann (1995), using dual somatic–dendritic and somatic–axonal recordings from neocortical layer V pyramidal neurons, provided the first evidence that  $I_{\text{NaP}}$  is likely to come from the soma or axon. Subsequently, several patch-clamp studies have supported a perisomatic distribution of  $I_{\text{NaP}}$  in layer 5 neocortical neurons of the somatosensory (Astman et al., 2006) and prefrontal cortex (Gonzalez-Burgos & Barrionuevo, 2001), and in CA3 (Urban et al., 1998) and CA1 pyramidal neurons (Andreasen & Lambert, 1999; Yue et al., 2005; Vervaeke et al., 2006).

However, dendritic exploration with patch-clamp electrodes revealed that  $I_{\text{NaT}}$  is also distributed along the apical trunk of pyramidal neurons at about the same density as in the soma membrane (Stuart & Sakmann, 1994; Magee & Johnston, 1995). The dendritic localization of  $I_{\text{NaT}}$ , together with the hypothesis that  $I_{\text{NaP}}$  and  $I_{\text{NaT}}$  arise from the same channel type, prompted groups to explore whether there is a functionally active  $I_{\text{NaP}}$  in the dendrites. Studies by Schwandt & Crill (1995) and Lipowsky et al. (1996) suggested such a dendritic localization in

both CA1 hippocampal and layer V neocortical pyramidal neurons. How can these results be explained in view of the abundant evidence for a perisomatic localization of  $I_{\text{NaP}}$ ? Schwandt & Crill (1995) iontophoretically applied glutamate to the dendrites while recording EPSCs at the soma, and found that bath-applied TTX reduced the EPSC amplitude. Lipowsky et al. (1996) activated excitatory synapses impinging on the distal dendrites. Because local application of TTX to the dendrites reduced the somatic EPSPs, they proposed that  $I_{\text{NaP}}$  in the dendrites boosted the EPSPs. However, an alternative explanation of the results from these two groups may be that dendritic regenerative  $\text{Na}^+$  spikes, carried by  $I_{\text{NaT}}$  in the dendrites, are caused by nearly synchronous synaptic activation of several dendritic spines onto a dendritic branch (Losonczy & Magee, 2006). Because these dendritic  $\text{Na}^+$  spikes are strongly filtered on their way along the dendrite and mostly fail to invade the soma, they will merely produce larger somatic EPSPs, with a slightly steeper rising slope that can easily remain undetected (Losonczy & Magee, 2006). Therefore, dendritic application of TTX that blocks local dendritic  $\text{Na}^+$  spikes will reduce the somatic EPSP amplitude. This scenario may explain why these two groups found a TTX-mediated decrease of synaptic potentials recorded at the soma.

Our work in CA1 pyramidal neurons further supports a perisomatic localization of  $I_{\text{NaP}}$  (Vervaeke et al., 2006). When we applied a voltage step that was just below the spike threshold (from  $-78$  to  $-58$  mV) during somatic whole-cell recording (Fig. 2B), thus activating  $I_{\text{NaP}}$  (Fig. 2A) but not  $I_{\text{NaT}}$ , we recorded a TTX-sensitive inward current ( $\sim 35$  pA) with very fast kinetics. Both the activation and deactivation could be fitted with single exponential functions with time constants of about 1 ms (Fig. 2B). These fast kinetics constrain the possible subcellular localization of  $I_{\text{NaP}}$ . Using detailed compartmental models of a CA1 pyramidal neuron based on reconstructed morphologies (Fig. 2C), we tested various possible subcellular localization of  $I_{\text{NaP}}$ , trying to reproduce the experimental results (Fig. 2D) (unpublished work). We found that  $I_{\text{NaP}}$  had to be localized in the immediate vicinity of the soma to reproduce the experimental results of Fig. 2B (Fig. 2D, dotted-dashed line). In comparison, distributing  $I_{\text{NaP}}$  (1) uniformly over soma and dendrites (Fig. 2D, continuous line), or (2) most of  $I_{\text{NaP}}$  at the axon initial segment and a much lower, uniform density in soma and dendrites (Fig. 2D, dashed line), or (3) most of  $I_{\text{NaP}}$  in the axon initial segment and a much lower density in the dendritic tuft (Fig. 2D, dotted line), all gave poor results. The model of  $I_{\text{NaP}}$  followed an activation curve as shown in Fig. 2A and had a voltage-independent time constant of 1 ms. In the model, fitting the  $I_{\text{NaP}}$  activation response with all  $I_{\text{NaP}}$  located in the axon initial segment (Fig. 2D, black trace) gave a somatic activation time constant of 1.07 ms, indicating a very good clamp control over  $I_{\text{NaP}}$ . These results strongly suggest that most of the channels underlying  $I_{\text{NaP}}$  are located very close to the soma.

Our results from hippocampal CA1 pyramidal cells are in good agreement with recent results from layer V pyramidal neurons by Astman et al. (2006), who provide strong evidence that  $I_{\text{NaP}}$  is specifically located at the axon initial segment. So why is the  $I_{\text{NaP}}$  conductance concentrated here, while there is hardly any

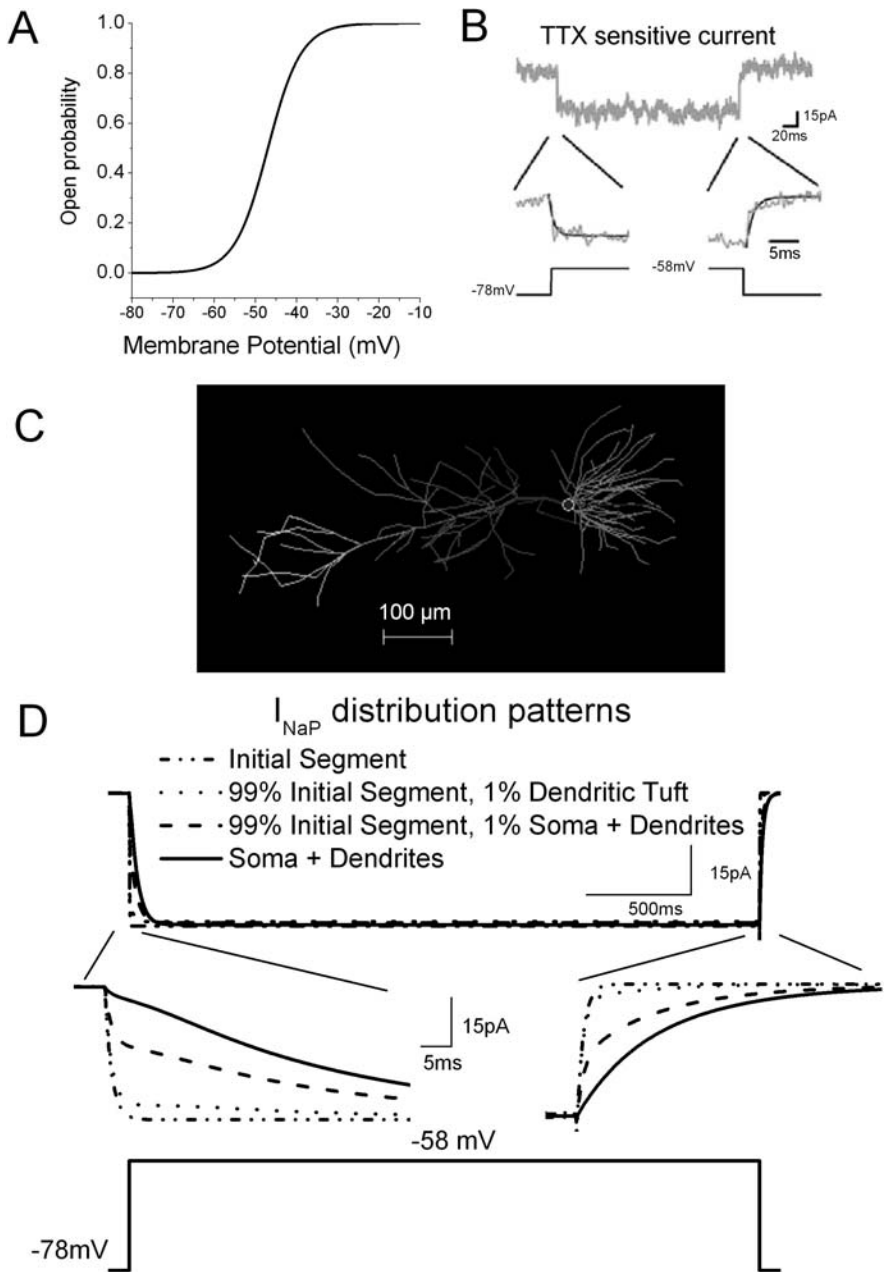


**Fig. 2** Computer simulations support that  $I_{NaP}$  largely originates from the axon initial segment of CA1 pyramidal neurons. (A)  $I_{NaP}$  steady-state activation curve used in the model and dynamic-clamp experiments. (B) Experimental data from a somatic whole-cell recording. The membrane potential was stepped from  $-78$  to  $-58$  mV. The gray trace shows the TTX-sensitive current obtained by subtraction the resulting currents of before and after

in the dendrites? A plausible answer to this question may be obtained by combining recent results on the subcellular distribution of  $I_{\text{NaT}}$  in cortical pyramidal neurons, with data on the molecular identities of  $\text{Na}^+$  channels in various parts of these cells. A recent elegant study by Kole et al. (2008) shows that the density of sodium channels underlying  $I_{\text{NaT}}$  is far higher (probably  $\sim 50$  times) in the axon initial segment than in the soma and dendrites of layer V pyramidal neurons. Thus, the subcellular distribution of  $I_{\text{NaT}}$  seems to match that of  $I_{\text{NaP}}$ , both being highly concentrated at the axon initial segment. This fits nicely with the evidence that  $I_{\text{NaP}}$  is at least partially caused by the same channels as  $I_{\text{NaT}}$ , probably through incomplete inactivation and/or a modal gating (Alzheimer et al., 1993; Taddese & Bean, 2002). Because the  $I_{\text{NaP}}$  in pyramidal cells is usually only a small fraction (typically  $\sim 1\%$ ) of  $I_{\text{NaT}}$  (French et al., 1990; Hu et al., 2002; Yue et al., 2005), the channel states generating  $I_{\text{NaP}}$  must occur very infrequently. This, combined with the far lower density of  $\text{Na}^+$  channels and  $I_{\text{NaT}}$  in the soma and dendrites compared to the axon, may partly explain why the density of  $I_{\text{NaP}}$  in the dendrites appears to be quite low. In addition, there is substantial evidence that that  $I_{\text{NaT}}$  in the axon initial segment and  $I_{\text{NaT}}$  in the soma and dendrites of pyramidal neurons are caused by channels of different molecular compositions (Kaplan et al., 2001; Boiko et al., 2001, 2003; Komai et al., 2006; Kole et al., 2008). Thus, in adult animals, axonal  $\text{Na}^+$  channels contain  $\alpha$ -subunits of the  $\text{Na}_v1.6$  type, whereas somatodendritic  $\text{Na}^+$  channels seem to be composed mainly of  $\text{Na}_v1.2$   $\alpha$ -subunits, perhaps in combination with  $\text{Na}_v1.1$  and  $\text{Na}_v1.3$  (Kaplan et al., 2001; Boiko et al., 2001, 2003; Kole et al., 2008). This also seems to fit in with data from transgenic mice indicating that  $I_{\text{NaP}}$  in several neurons is to a large extent ( $\sim 40$ – $70\%$ ) mediated by  $\text{Na}_v1.6$   $\alpha$ -subunits, e.g., in Purkinje and mesencephalic trigeminal neurons, although other  $\alpha$ -subunit species can also contribute to  $I_{\text{NaP}}$  (Raman & Bean, 1999; Enomoto et al., 2007; Taddese & Bean, 2002). Thus, the  $I_{\text{NaP}}$  of pyramidal neurons may be largely caused by  $\text{Na}_v1.6$ -containing  $\text{Na}^+$  channels concentrated at the axon initial segment, both because of the very high channel density here and the  $\text{Na}_v1.6$  subunits are especially prone to the particular gating mode that generates  $I_{\text{NaP}}$ . In addition, certain  $\text{Na}^+$  channel  $\beta$ -subunits may also enhance  $I_{\text{NaP}}$  (Qu et al., 2001).



**Fig. 2** (continued) TTX application. (Modified from Vervaeke et al., 2006, with permission from *Cell Press, Elsevier*.) **(C)** Reconstructed neuron used for the simulations in **(D)**. Different shades of gray indicate different membrane potentials during a simulation where the soma was clamped at  $-58$  mV. **(D)** The experiment in **(B)** was simulated with various  $I_{\text{NaP}}$  distribution patterns, as indicated. *Continuous line*:  $I_{\text{NaP}}$  was uniformly distributed in soma and dendrites ( $0.325$  pS/ $\mu\text{m}^2$ ). *Dot-dash line*: all  $I_{\text{NaP}}$  ( $50$  pS/ $\mu\text{m}^2$ ) was located in the axon initial segment. *Dashed line*: most of  $I_{\text{NaP}}$  ( $99\%$ ) was located in the axon initial segment ( $20.5$  pS/ $\mu\text{m}^2$ ) while the density was 100 times lower ( $1\%$ ) in soma and dendrites ( $0.205$  pS/ $\mu\text{m}^2$ ). *Dotted line*: most of  $I_{\text{NaP}}$  ( $99\%$ ) was located in the axon initial segment ( $45$  pS/ $\mu\text{m}^2$ ) while the density was 100 times lower ( $1\%$ ) in the distal dendritic tuft ( $0.45$  pS/ $\mu\text{m}^2$ ). (K. Vervaeke, unpublished.)

### 3.3 Further Advantages of Dynamic Clamp

The fact that a dynamic-clamp system can cancel or restore  $I_{\text{NaP}}$  nearly instantaneously is a very important advantage compared to application of ion channel blockers or openers, which usually require several minutes to take full effect. During such a long delay, access resistance, neuronal, and/or network properties may change, thus complicating the interpretation of the results.

Furthermore, by using dynamic-clamp  $I_{\text{NaP}}$  can be increased or decreased in an arbitrary graded fashion, allowing the parameters of the  $I_{\text{NaP}}$  model to be varied freely, e.g., to resemble natural modulation (Astman et al., 1998; Cantrell & Catterall, 2001; Rosenkranz & Johnston, 2007). Also, because a given manipulation with dynamic clamp is instantaneous and does not require pharmacologic blockers, it is well suited for in vivo patch-clamp recordings. This would be especially important for studying  $I_{\text{NaP}}$  function in neurons embedded in an active network, e.g., during responses to sensory stimuli.

## 4 Methods Used for Studying $I_{\text{NaP}}$ Functions by Dynamic Clamp

### 4.1 Characterization of $I_{\text{NaP}}$ for Modeling and Dynamic Clamp

In order to establish our dynamic clamp for manipulating  $I_{\text{NaP}}$ , we first needed to determine its steady-state activation curve in CA1 hippocampal pyramidal cells, for building an accurate model of the current. For this purpose, we used two types of measurements (Hu et al., 2002), both obtained by whole-cell recording from the soma of this cell type in hippocampal slices from young male rats, under virtually identical experimental conditions as those used in the main study (Vervaeke et al., 2006).

We used voltage-clamp recording of the current (Hu et al., 2002) evoked by a slow voltage ramp (from  $\sim -90$  to  $\sim -30$  mV; Fig. 3A) before and after blockade of  $I_{\text{NaP}}$  by TTX. The TTX-sensitive current obtained by subtracting the two current recordings started to activate between  $-70$  and  $-65$  mV (Fig. 3B). A similar activation curve was obtained by a series of depolarizing voltage-clamp steps before and after TTX application (Fig. 3C–E). Both these methods yielded similar results (Hu et al., 2002), which also agree well with previous experimental reports from CA1 hippocampal pyramidal cells and other neurons (French et al., 1990; Crill, 1996).

To assess the time constants of  $I_{\text{NaP}}$  activation and deactivation in the subthreshold voltage range, somatic whole-cell voltage-clamp measurements were used (Fig. 2B). A 250-ms-long voltage step from  $-78$  to  $-58$  mV was applied and the clamp current before and after TTX application subtracted to obtain  $I_{\text{NaP}}$ . The activation and deactivation time courses of  $I_{\text{NaP}}$  were each

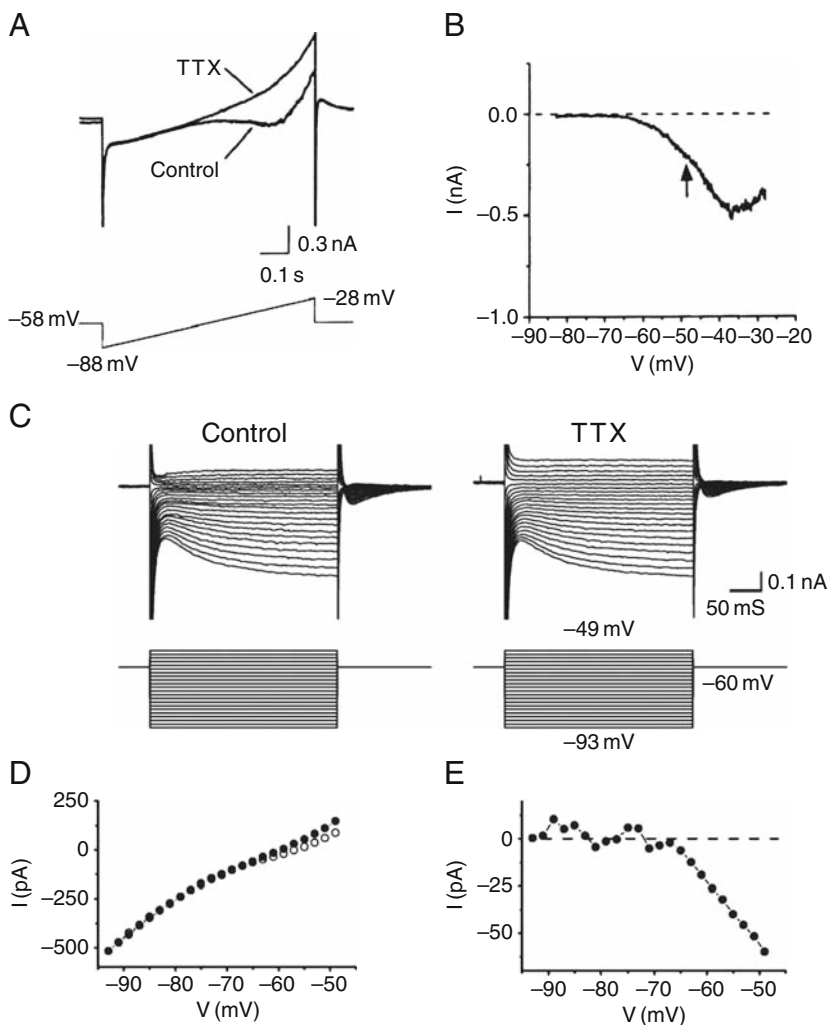


**Fig. 3** Voltage-clamp measurements of  $I_{NaP}$  in of CA1 pyramidal neurons. (A) Membrane currents in response to a ramp voltage command (from  $-88$  to  $-28$  mV) before and after application of TTX ( $1 \mu\text{M}$ ). (B) Voltage dependence of the TTX-sensitive current ( $I_{NaP}$ ) obtained by subtracting the current in response the ramp command before and after TTX application. The arrow indicates the action potential threshold for this cell. (C) Membrane currents in response to voltage-clamp steps to different membrane potentials (from  $-93$  mV to  $-40$  mV) before and after TTX application. (D) Steady-state current-voltage ( $I-V$ ) plot of the data from (C), measured at the end of the voltage steps. (E) TTX-sensitive current ( $I_{NaP}$ ), calculated by subtracting the steady-state currents before and after TTX in (C). Note that the  $I_{NaP}$  started to activate at about  $-65$  mV in both (B) and (E). (Modified from Hu et al., 2002, with permission from *The Journal of Physiology*, Wiley-Blackwell.)

fitted with a single exponential function. The best fits had time constants of  $\sim 1$  ms (0.93.14 and  $0.99 \pm 0.15$  ms, respectively). Therefore, voltage-independent activation and deactivation time constants of 1 ms were used for our  $I_{\text{NaP}}$  model and dynamic clamp.

## 4.2 Na<sup>+</sup> Current Models Used for Our Dynamic Clamp and Computational Modeling

Next, we applied the model of  $I_{\text{NaP}}$  in a detailed model of a CA1 pyramidal cell that we have developed over the last decade, in agreement with the available voltage- and current-clamp data (Borg-Graham, 1999; Shao et al., 1999; Vervaeke et al., 2006). Like in these previous studies, we modeled the total Na<sup>+</sup> current as a sum of two components:  $I_{\text{NaT}}$  represented by a four-state Markov model and  $I_{\text{NaP}}$  represented by a HH model (Borg-Graham, 1999). For our dynamic clamp, we used the same HH model of  $I_{\text{NaP}}$ , which reproduced the main features of experimental voltage-clamp recordings of  $I_{\text{NaP}}$  in rat CA1 pyramidal cells (Figs. 3 and 4A,C) as well as those of  $I_{\text{NaP}}$ -dependent responses to subthreshold current ramps (Figs. 4B, 5, 6, and 7). The motivation for the use of the new Markov model, rather than the classical HH model of the entire Na<sup>+</sup> current was based on the following considerations.

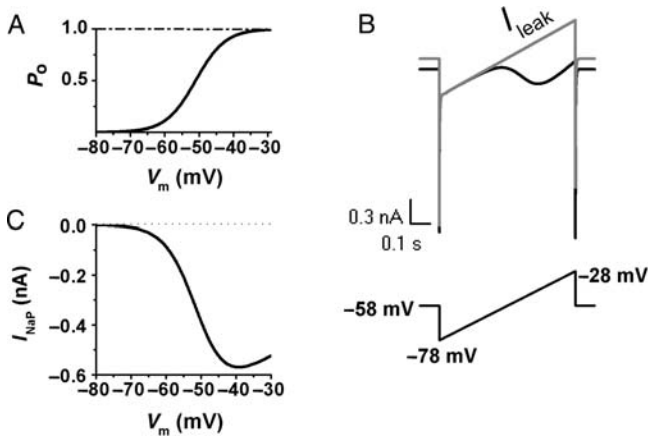


**Fig. 4 Properties of the  $I_{\text{NaP}}$  model used for our dynamic clamp.** Model simulations of  $I_{\text{NaP}}$  under voltage clamp. (A) Steady-state activation curve of the  $I_{\text{NaP}}$  model.  $P_o$  is the open probability. The voltage-independent activation and deactivation time constant was 1.0 ms. (B)  $I_{\text{NaP}}$  (black) compared to leak current (gray) in response to a voltage ramp command (lower trace) in the model. (C)  $I_{\text{NaP}}$  obtained by subtracting the current responses shown in (B). (Modified from Vervaeke et al., 2006, with permission from *Cell Press, Elsevier*.)

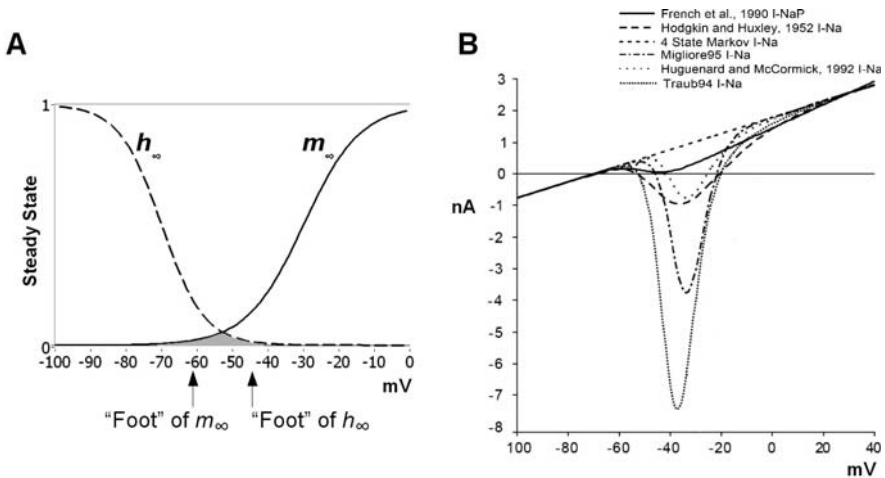


**Fig. 5 Window current and steady-state characteristics of Hodgkin-Huxley (HH) Na<sup>+</sup> channel models.** (A) The HH model of  $I_{Na}$  is defined in part by the voltage-dependent steady-state values of activation and inactivation ( $m_\infty$  and  $h_\infty$ ). Although the current is nominally transient, this model predicts a nonzero steady-state current for voltages where the two curves overlap (*gray region*), giving what is called the HH “window current.” The positions on the voltage axis for the “feet” of these curves may be directly related to transient, e.g., firing, properties of  $I_{Na}$  including the span of spike thresholds and the minimum pre-hyperpolarization (PHP), before a spike that is required to remove inactivation. (B) Steady-state  $I$ - $V$  characteristics of different Na<sup>+</sup> channel HH models (squid axon: Hodgkin & Huxley, 1952; hippocampal pyramidal cell: Traub et al., 1994, and Migliore et al., 1995; thalamic relay cell model adapted from cortical pyramidal cells: McCormick & Huguenard, 1992) inserted in a passive cell model, compared with the measured values of  $I_{NaP}$  (hippocampal pyramidal cell: French et al., 1990), showing that the steady-state inward rectification predicted by these models are much larger than the actual  $I_{NaP}$ . The modified four-state Markov model used in this study shows a negligible steady-state inward rectification

#### 4.2.1 HH Models and $I_{NaP}$ , and the Necessity of a New $I_{Na}$ Model

The standard approach for modeling macroscopic neuron currents follows the paradigm established by Hodgkin & Huxley (1952) for Na<sup>+</sup> and K<sup>+</sup> currents in the squid axon. Nevertheless, this formalism fails to account for various properties of currents in other preparations, including hippocampal pyramidal cells (Borg-Graham, 1987; Kuo & Bean, 1994). Here we describe these limitations with respect to the Na<sup>+</sup> current, and how we addressed them in the theoretical foundation of our study of  $I_{NaP}$ .

The HH Na<sup>+</sup> channel model includes activation,  $m$ , and inactivation,  $h$ , “gating particles” whose voltage-dependent kinetics are defined in part by sigmoidal functions of their steady state,  $m_\infty$  and  $h_\infty$ , respectively, parameterized by the position and steepness on the voltage axis. Any overlap of the  $m_\infty$  and  $h_\infty$  functions in the HH model predicts a steady state, or noninactivating,

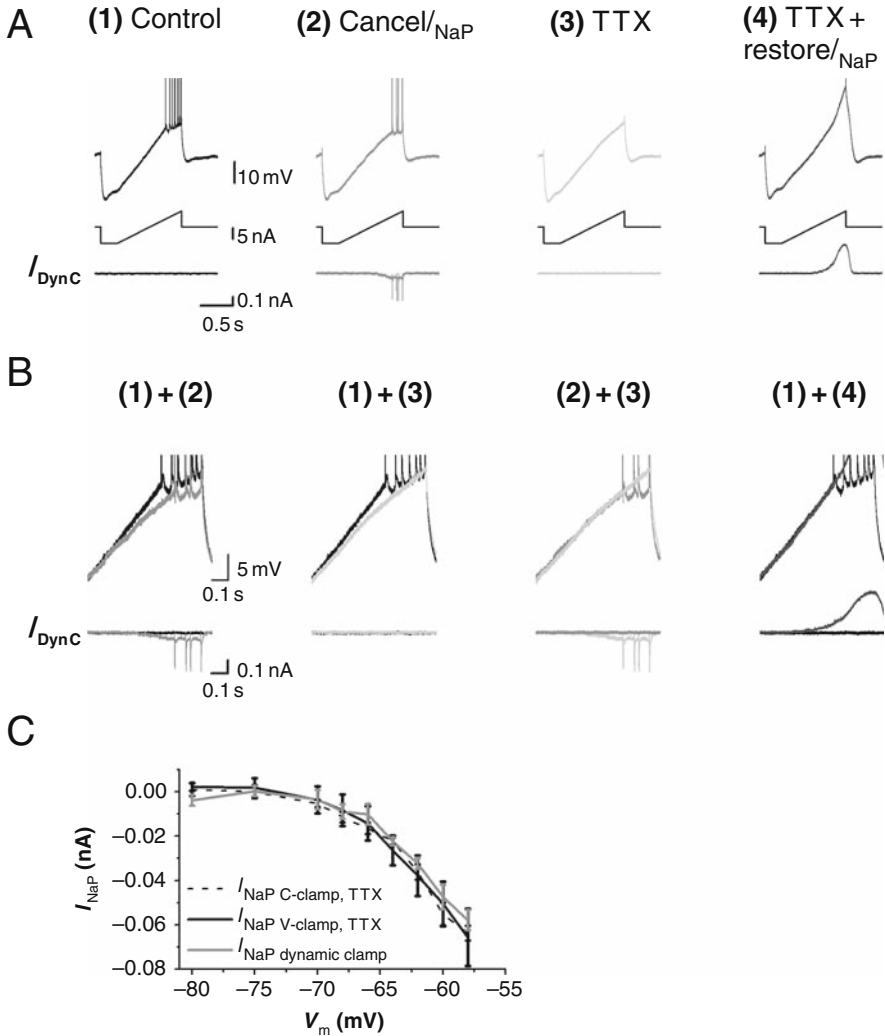


**Fig. 6** Comparing the effects of effects of  $I_{NaP}$  subtraction by dynamic clamp with effects of  $I_{NaP}$  blocked by TTX. **(A)** voltage responses to a current ramp before (1) and after (2) canceling  $I_{NaP}$  with dynamic clamp, followed by application of 1  $\mu$ M TTX and dynamic clamp turned off (3) and after restoring  $I_{NaP}$  with dynamic clamp in the presence of TTX (4). These four conditions were executed in sequence in each cell. The bottom traces show the current output from the dynamic clamp ( $I_{DynC}$ ). **(B)** The same traces as in (A) shown superimposed on expanded scales. **(C)** Voltage dependence of  $I_{NaP}$ . Summary plots from three types of measurements: (1) the subthreshold TTX-sensitive current obtained in voltage clamp (V-clamp, TTX;  $n = 5$ ; data from Hu et al., 2002), (2) the TTX-sensitive subthreshold current obtained from current-clamp recordings as shown in panel (B) and in Fig. 7 (C-clamp, TTX;  $n = 5$ ), and (3) the artificial  $I_{NaP}$  produced by our dynamic clamp ( $n = 5$ ). (Modified from Vervaeke et al., 2006, with permission from *Cell Press, Elsevier*.)

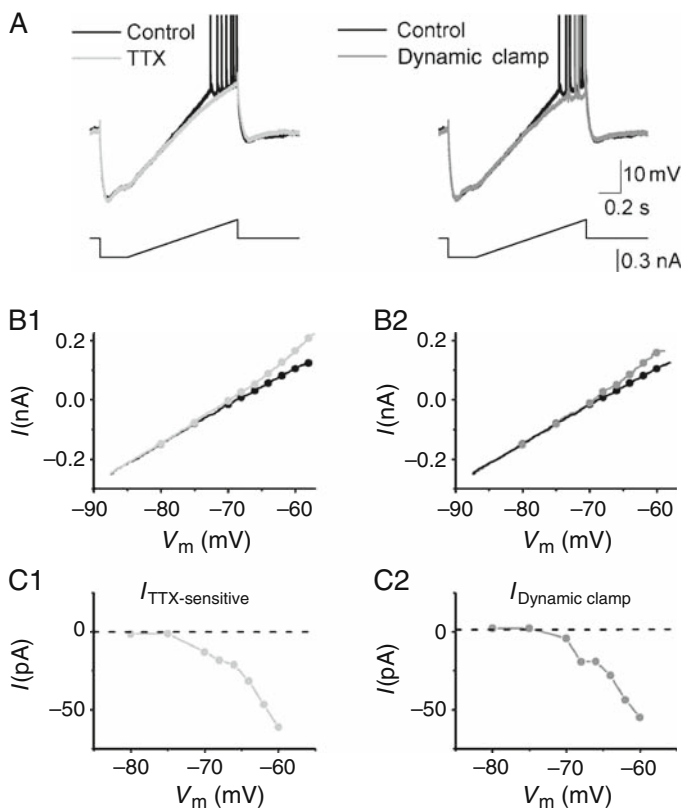


**Fig. 7 Method for determining the voltage-dependence of  $I_{\text{NaP}}$  from current clamp data.** (A) A current ramp (bottom traces) was injected into the cell and the voltage response recorded before and after application of TTX (left) or before and after applying dynamic clamp (right). During the subthreshold parts of the responses, every value of injected current ( $I$ ) corresponds to a certain value of the membrane potential ( $V_m$ ). (B1, B2) The values of injected current ( $I$ ) and  $V_m$ , taken from (A) are re-plotted, by plotting  $I$  as a function of  $V_m$ . (C1) and (C2) show the differences of the plots within B1 and B2, respectively, thus revealing the voltage dependence of the TTX-sensitive sub-threshold current,  $I_{\text{NaP}}$  (C1) and dynamic clamp current (C2). (Modified from Vervaeke et al., 2006, with permission from *Cell Press, Elsevier*.)

component – or “window current” – of this nominally transient current (Fig. 5A), which is kinetically indistinguishable from a true persistent  $\text{Na}^+$  current. Thus, measurement of a noninactivating  $\text{Na}^+$  current sets an upper bound on the HH model window current, which in turn constrains the overlap of the  $m_\infty$  and  $h_\infty$  curves. At the same time, the positions and slopes of  $m_\infty$  and  $h_\infty$  are constrained by quantitative aspects of firing, and the key question is whether the HH model of the  $\text{Na}^+$  current can satisfy all the constraints.

Here we focus on how two measures of spike firing in pyramidal neurons constrain  $m_\infty$  and  $h_\infty$ , including the range of thresholds (roughly between  $-60$  and  $-50$  mV), and the maximum hyperpolarization between

spikes during repetitive firing (around  $-60$  mV). To simplify matters, we can neglect any voltage dependence of the HH model time constants, as well as the number of  $m$  or  $h$  particles (for more than one particle, the relevant sigmoid function describes the steady-state value of the ensemble). Thus, the lowest spike threshold of around  $-60$  mV imposes an upper bound on the “foot” of the  $m_\infty$  curve, since a sufficient number of  $I_{\text{Na}}$  channels must be activated for triggering an action potential (Fig. 5A). Next,  $I_{\text{Na}}$  channels are inactivated during a spike, and thus to allow a subsequent spike, such as during repetitive firing, the membrane voltage must become low enough to remove this inactivation. This means that the lowest voltage between spikes imposes a lower bound on the “foot” of the  $h_\infty$  curve. This potential was termed the “PHP,” or “pre-hyperpolarization” in (Borg-Graham, 1987), in contrast to “AHP” since the PHP is functionally related to a spike which follows, not precedes, it.

These quantitative constraints are susceptible to the subcellular distribution of the channels, in that a given measured voltage (typically at the soma) may differ from the voltage “seen” by the channel. Nevertheless, as argued in our earlier work (Borg-Graham, 1987), the main point is that measured properties of hippocampal pyramidal cells constrain the  $m_\infty$  and  $h_\infty$  curves of the HH model to predict a window current that is at least an order of magnitude larger than direct measurements of  $I_{\text{NaP}}$ . This can be seen in Fig. 5B, where we compare the steady-state properties of  $I_{\text{NaP}}$  predicted by various published models of hippocampal pyramidal cells and other neurons, as well as the canonical HH squid axon parameters (adjusted for cell input impedance). In this comparison the maximum conductance of each  $I_{\text{Na}}$  model was adjusted so that they would give approximately the same spike current. Although this gives a relatively crude quantitative comparison (apart from amplitude, there was no detailed fitting of spike), it is clear that the HH-type  $I_{\text{Na}}$  models predict a wide range of persistent  $\text{Na}^+$  currents, all of which overestimate the true  $I_{\text{NaP}}$ . This implies not only important differences between the models regarding synaptic integration and firing properties, but also, given our results with  $I_{\text{NaP}}$ , predictions at odds with the behavior of real neurons.

### An Ad Hoc Markovian Model

Being more flexible, general Markov-type models can meet constraints which are impossible for the standard HH paradigm (ref. Kuo & Bean (1994) from hippocampus; Vandenberg & Bezanilla (1991) and Patlak (1991) from squid axon). A previous approach was to fit more than one HH-type model (Borg-Graham, 1987), each with relatively nonoverlapping activation and inactivation curves in order to limit the window current of  $I_{\text{Na}}$ , and whose voltage dependences spans a range sufficient to account for the observed range of spike thresholds. Note that this approach can be reduced to an equivalent, if complex, single Markov model; an advantage with considering “separate” channels is

that it can facilitate the initial fitting to desired kinetics. On the other hand, there is no data to support such kinetically distinct  $\text{Na}^+$  channels.

Borg-Graham (1999) proposed a new ad hoc Markovian model for  $I_{\text{Na}}$  that was consistent with qualitative aspects of channel gating established from single-channel studies, and quantitative constraints inferred from macroscopic properties of the sodium current during action potentials. The model had two key predictions. First, the activation–inactivation sequence of the channel during and after a spike was dominated by a one-way path between an inactivated state,  $I$ , a closed state,  $C$ , an activated, open (conducting) state,  $O$ , and then back to the inactivated state. The implicit constraint that inactivation necessarily followed activation had been shown by single-channel studies (Armstrong, 1981; Patlak, 1991; Kuo & Bean, 1994). The second explicit prediction of the model was that the voltage-dependent transition rate from the  $C$  state to the  $O$  state took into account the history of the membrane voltage. Thus, from the  $C$  state, as the membrane voltage increased, equilibrium increasingly favored the  $O$  state, following a monotonic function of voltage parametrized by a reference voltage  $V_{C-O}$ . On the other hand, if the membrane voltage decreased, the voltage dependence of  $C$ – $O$  transition itself shifted to more hyperpolarized voltages, specifically, the value of  $V_{C-O}$  also decreased. In the basic form of the model the hyperpolarization of  $V_{C-O}$  with membrane hyperpolarization is irreversible (the time constant for any rightward shift of  $V_{C-O}$  with depolarization was infinite), though the scheme can easily incorporate, e.g., a slow adaptation of threshold following a slow depolarization of the membrane voltage. For convenience, the actual model used in the current study encapsulates the kinetics of the  $C$ – $O$  transition described above with two distinct  $C$  states, but the qualitative behavior is similar. In sum, this model provides both a significant range of spike thresholds, where the dynamic spike threshold has an intrinsic memory of subthreshold potentials. Threshold is lower for lower previous membrane voltages, such as for the first spike of a train arising from rest, as compared to later spikes. Since the minimum membrane voltage, or PHP, between spikes in a train (for pyramidal cells) is many millivolts above rest, and since threshold depends on the PHP, the model predicts that thresholds for later spikes are higher than that for the first spike. Note that the proposed mechanism is not a *necessary* condition for a nonzero range of thresholds nor dependence on voltage history – even the original squid axon model of HH will show some degree of these characteristics. However, in principle the new Markov  $I_{\text{Na}}$  model can better account for the quantitative aspects of these characteristics, in part because it is explicitly formulated to account for these properties, as opposed to a model where these properties are more emergent due to interactions between  $\text{Na}^+$  and  $\text{K}^+$  currents.

Unlike the HH formalism, this scheme allows essentially independent parameter fitting to the transient and steady-state properties of the  $\text{Na}^+$  current. Specifically, realistic spike threshold dynamics can be reproduced given an essentially arbitrary steady-state value of the  $O$  state, that is a persistent

component of the  $\text{Na}^+$  current. In the original version of the model, this aspect was adjusted to match published data on  $I_{\text{NaP}}$ , thus the defined  $I_{\text{Na}}$  accounted for all the  $\text{Na}^+$  current, transient and persistent. Note that the HH model not only predicts a very large maximum window current: Since this model predicts complete inactivation with increased depolarization ( $h_\infty$  goes to zero), the HH window conductance approaches zero with increased depolarization. The experimentally measured persistent  $\text{Na}^+$  current, however, shows a relatively constant conductance above the voltage for full activation. Although the functional effect of this relatively small current during the spike is unclear, the proposed Markov model of the entire  $\text{Na}^+$  current can, in fact, reproduce this aspect. This result also confirms that an HH model, strictly speaking, cannot by itself account for the measured  $I_{\text{NaP}}$ .

As described earlier, for convenience and clarity in the present work, the original ad hoc Markov model was adjusted to have a negligible steady-state component, and a distinct  $I_{\text{NaP}}$  was explicitly modeled with a separate non-inactivating HH-type model. Nevertheless, from a kinetic standpoint, the complete Markov model and the hybrid Markov and HH model formulations are identical.

### ***4.3 Dynamic-Clamp Configuration for Analysis of $I_{\text{NaP}}$ Functions***

Figure 1 shows a diagram of the dynamic-clamp configuration that we have used in our studies of  $I_{\text{NaP}}$  functions in rat CA1 pyramidal cells. We used two separate patch pipettes, both in whole-cell configuration at the soma of the same cell: one pipette for voltage recording, the other for current injection. The pipettes were coupled to a *DynClamp2* dynamic-clamp system (Pinto et al., 2001), which has an update rate of about 10 kHz ( $\Delta t \sim 100 \mu\text{s}$ ) and was run on a *Pentium IV* computer with a *Digidata 1200* as ADC–DAC board (Molecular Devices). For every cycle, the expected amplitude of  $I_{\text{NaP}}$  was calculated by the dynamic-clamp software, based on our  $I_{\text{NaP}}$  model and the measured membrane potential. To cancel the intrinsic  $I_{\text{NaP}}$  generated by the neuron itself, a negative current equal to the simulated  $I_{\text{NaP}}$  was injected into the cell in real time. To add  $I_{\text{NaP}}$  after blocking the native persistent  $\text{Na}^+$  current by TTX, a positive current equal to the simulated  $I_{\text{NaP}}$  was injected into the cell.

### ***4.4 Advantages of Using Two Separate Electrodes for Dynamic Clamp***

During dynamic clamp, it is necessary to measure the membrane potential very accurately and at the same time pass considerable amounts of current into the

cell. If the same patch pipette is used for both the voltage recording and current injection, a voltage error occurs due to the voltage drop caused by current flowing across the series or access resistance, ( $R_s$ ), across the electrode. Thus, without compensation, the recorded voltage is the sum of the true membrane potential and the voltage drop across series resistance. Although most intracellular amplifiers use a subtraction technique known as “bridge balance” to eliminate the voltage drop caused by series resistance, this compensation is performed manually and is never perfect. Furthermore, the series resistance can often vary spontaneously during a recording, causing errors in the compensation. Thus, a series resistance that is not completely compensated may cause significant voltage errors, particularly when large currents are injected through the recording electrode, for instance, when using dynamic clamp to cancel or mimic the currents underlying action potentials (Ma & Koester, 1996). Since the reliability of dynamic clamp critically depends on the accuracy of the voltage measurements that are fed into the computer that calculates the output clamp current, and the clamp current often depends steeply and nonlinearly on the voltage, it is essential to avoid voltage recording errors. Therefore, we took special care to minimize the voltage recording error in our study of  $I_{NaP}$ , by using separate voltage recording and current injection pipettes (Fig. 1). We found that this was a significant advantage, because even though the amplitude of  $I_{NaP}$  in CA1 pyramidal is relatively small ( $\sim 0.1$ – $0.5$  nA; Fig. 2) compared with the current underlying the action potential, it activates steeply over a narrow voltage range and has quite fast kinetics, so that even small voltage errors may have significant consequences.

For example, assuming that  $I_{NaP}$  is 0.5 nA (Fig. 3A), and the true series resistance  $R_s = 20$  M $\Omega$ , a 10% error in the bridge balance, or a 10% change in  $R_s$  (2 M $\Omega$ ), will give a voltage error of about 1 mV. This error in turn will cause an error in the injected  $I_{NaP}$ . Although small, this difference may still significantly affect spike timing in response to ramps and noisy inputs close to the spike threshold because of the regenerative nature of  $I_{NaP}$ , and the fact that the spike threshold is close to the half activation potential of  $I_{NaP}$ , thus where its activation curve is steepest (Fig. 2A). Furthermore, it is not uncommon that the series resistance is larger than 20 M $\Omega$ , and the bridge compensation error may exceed 10%, causing more severe distortions.

The same technique was also used in a recent paper to study the contribution of Kv3 channels to action potential repolarization and high-frequency firing in hippocampal interneurons (Lien & Jonas, 2003). Although powerful, the application of this multiple electrodes recording method is largely limited by the difficulty of obtaining two nearby (preferentially within about 20  $\mu$ m) simultaneous recordings from same neuron (Williams, 2004).

In addition to the voltage drop error induced when the current is supplied with the same electrode that monitors the voltage, the series resistance, in combination with the capacitance of the recording pipette, acts as a low-pass filter, decreasing the amplitude of fast voltage signals (i.e., action potentials) even when the two-electrode configuration is used. Therefore, we constantly

compensated the series resistance of the voltage recording electrode during each recording, and rejected experiments on which the series resistance was too high.

Although there is a clear advantage of using two electrodes, it is also possible to use dynamic clamp in combination with single electrode recording, where the same pipette is used for both voltage recording and current injection. In a few of our experiments on  $I_{\text{NaP}}$  functions we also used this configuration (see Fig. 5 in Vervaeke et al., 2006). This possibility is of course essential for using dynamic clamp for in vivo experiments.

#### 4.5 Testing and Adjusting Our Dynamic-Clamp Parameters

Before using our dynamic clamp for functional studies, we tested its performance in pilot experiments, starting with a maximal conductance for  $I_{\text{NaP}}$  ( $G_{\text{max}}$ ) value of  $\sim 5$  nS, which was determined from previous voltage-clamp data (Hu et al., 2002). Next, we adjusted this value after comparing the effects of  $I_{\text{NaP}}$  subtraction by the dynamic clamp, with the effects of blocking  $I_{\text{NaP}}$  with TTX (Fig. 6).

In these pilot experiments, we recorded responses of the cell to a slow, injected current ramp (Fig. 6A), and used the dynamic clamp to subtract  $I_{\text{NaP}}$ .  $G_{\text{max}}$  was then increased stepwise from the starting value, in steps of 0.4 nS, until we could reliably cancel the effect of the intrinsic  $I_{\text{NaP}}$  during the injected current ramp (Fig. 6A 1 – 2 and B 1 + 2) to the same extent as blockade by TTX (Fig. 6A 3 and B 2 + 3). We could then also fully restore the effect of the intrinsic  $I_{\text{NaP}}$  by dynamic clamp, after  $I_{\text{NaP}}$  had been blocked by TTX (Fig. 6A 4 and B 1 + 4). We found that the  $G_{\text{max}}$  value that could most reliably eliminate and restore  $I_{\text{NaP}}$  during our recordings was 4.8 nS. This value then was used for our subsequent experiments in this series (Vervaeke et al., 2006).

Figure 6C compares the voltage dependence plots of  $I_{\text{NaP}}$  obtained from the three different types of measurement: (1) the subthreshold TTX-sensitive current obtained in voltage clamp (V-clamp, TTX; data from Hu et al., 2002), (2) the TTX-sensitive subthreshold current obtained from current-clamp recordings as shown in Figs. 3B and 7, and (3) the artificial  $I_{\text{NaP}}$  produced by our dynamic clamp. The three types of measurement yielded virtually identical results.

To test the response speed of the dynamic-clamp system we applied a voltage step from  $-78$  to  $-58$  mV in the open loop configuration and fitted the response with single exponential functions, giving activation and deactivation time constants of 1.01 and 1.00 ms, respectively, as shown above (Fig. 3B).

To test the hypothesis that channels underlying  $I_{\text{NaP}}$  are localized near the soma, we used computational modeling, as already described above (Section 3.2; Fig. 2). To further test this hypothesis, we also used local application of TTX while giving subthreshold depolarizing voltage steps (from  $-78$  to  $-58$  mV, like in Fig. 2C) through a somatic recording electrode and monitoring the inward current. We then compared the effects of TTX applied locally to the soma with a micropipette (and a dye, 0.2 Vol% fast green, which showed that

the application spread  $\sim 100$   $\mu\text{m}$  perpendicular to the somatic layer), and subsequent bath application of TTX ( $1$   $\mu\text{M}$ ). There was no significant difference between these effects, and local puffing of TTX occluded the effect of subsequent bath application of TTX (data not shown; Vervaeke et al., 2006). These tests strongly support the conclusion that  $I_{\text{NaP}}$  is confined to the perisomatic area, probably mainly at the axon initial segment (Astman et al., 2006).

#### 4.6 Limitations of Our Dynamic-Clamp Approach

For our multicompartiment model of a CA1 pyramidal cell (Vervaeke et al., 2006), we have modeled the total  $\text{Na}^+$  current as a sum of two components, as described above:  $I_{\text{NaT}}$  represented by a four-state Markov model and  $I_{\text{NaP}}$  represented by a HH model (Borg-Graham, 1999), both  $I_{\text{NaT}}$  and  $I_{\text{NaP}}$  being confined to the soma, because there is good evidence for an extremely high  $\text{Na}^+$  channel density in the axon initial segment of cortical pyramidal cells (Kole et al., 2008). Our dynamic clamp was based on the same HH model of  $I_{\text{NaP}}$ . This is obviously a great simplification compared to a fully realistic model of the  $\text{Na}^+$  channels in this cell type, which is likely to comprise several molecular species, including the channels made by  $\text{Na}_v1.6$   $\alpha$ -subunits in the axon, and  $\text{Na}_v1.2$ , perhaps in combination with  $\text{Na}_v1.1$  and  $\text{Na}_v1.3$  distributed over the somatodendritic membrane. Each of these may be further diversified by various  $\beta$  subunits and by modulation; each channel species may switch between more than ten different states, which may lead to a continuum of biophysical properties for each type rather than merely two distinct currents  $I_{\text{NaT}}$  and  $I_{\text{NaP}}$  (see, e.g., Taddese & Bean, 2002). Thus, by necessity, the  $\text{Na}^+$  current models used in our CA1 cell model as well as in our dynamic clamp are obviously relatively simple approximations to the reality. Nevertheless, they reproduced and predicted important features of the cell's behavior, and our dynamic clamp was capable of both canceling and reproducing the main effects of the intrinsic  $I_{\text{NaP}}$  on somatic AHPs,  $f/I$  relation and, to some extent, spike timing. These observations suggest that these effects are fairly robust consequences of a subthreshold, voltage-dependent, persistent  $\text{Na}^+$  conductance, and therefore tend to occur independently of the finer details in the properties of the  $\text{Na}^+$  current.

Another major limitation of the HH model of  $I_{\text{NaP}}$  that we used for our dynamic clamp was that it did not include channel noise. Hence in our experiments we could not add noise caused by stochastic opening of simulated  $I_{\text{NaP}}$  channels. It has been suggested theoretically and supported by experimental evidence that ion channel noise can strongly affect spike time precision (Schneidman et al., 1998; White et al., 2000). Moreover, there is evidence that  $\text{Na}^+$  channel noise caused by  $I_{\text{NaP}}$  channels is essential for subthreshold oscillations in entorhinal stellate neurons (Dorval, Jr. & White, 2005). However, our recent results suggest that subthreshold oscillations in CA1 hippocampal cells depend not only on intrinsic channel noise but also on  $I_{\text{NaP}}$  as an amplification mechanism (see Section 5.2).

### 4.7 Comparing Model Simulations and Dynamic-Clamp Manipulation of $I_{NaP}$

Throughout our study, we compared simulations performed by computational modeling of a CA1 pyramidal cell with results from dynamic-clamp experiments and other experimental manipulations. In most cases, we used a relatively simple computational model (8 compartments, 11 conductances; Vervaeke et al., 2006), but in order to check our results with the simple model we also employed far more complex and detailed models, comprising several hundred compartments (Fig. 2C, unpublished). Figure 8 shows the responses of the simple eight-compartment model cell to a ramp current injection, similar to those performed experimentally (Figs. 6 and 7). Omission of  $I_{NaP}$  in the model (Fig. 8, no  $I_{NaP}$ ) had similar effects as canceling  $I_{NaP}$  with dynamic clamp or blocking it with TTX in real cells (Figs. 6 and 7).

### 4.8 Predictive Modeling

In our study of  $I_{NaP}$  functions in CA1 pyramidal cells (Vervaeke et al., 2006), we decided to test several of our ideas theoretically by computational modeling before testing the same ideas experimentally. Thus, we used our models to make predictions, before testing the predictions by intracellular recordings in brain slices with dynamic clamp, channel blockers, or other manipulations (Vervaeke et al., 2006). For example, our simulations led to the prediction that  $I_{NaP}$  would increase the amplitudes of AHPs (Fig. 9A). When we subsequently tested this prediction experimentally with dynamic clamp (Fig. 9B) or with TTX, the prediction was confirmed (Vervaeke et al., 2006); see Section 5.1, below). The

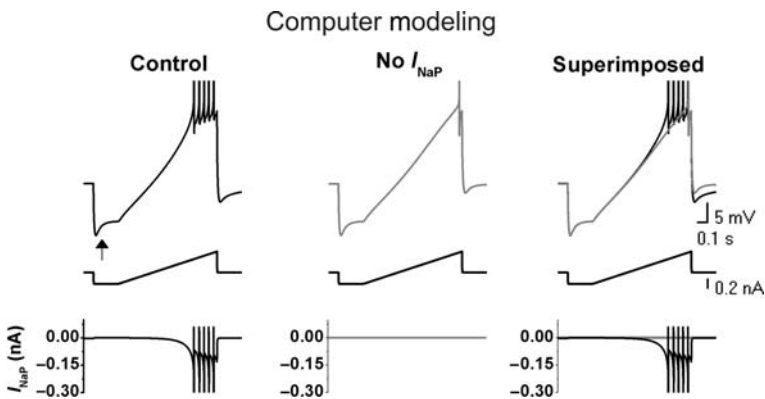


**Fig. 8 Model simulations of  $I_{NaP}$  in current clamp.** Voltage responses (upper traces) to a current ramp command with (black) and without  $I_{NaP}$  (gray). The time course of  $I_{NaP}$  is plotted below. (Modified from Vervaeke et al., 2006, with permission from *Cell Press, Elsevier*.)

model simulations also predicted that  $I_{\text{NaP}}$  would have contrasting effects on the excitability of the cell. As intuitively expected, the model predicted that  $I_{\text{NaP}}$  would reduce the minimal current necessary to evoke spiking (rheobase). In addition, however, the model also predicted that  $I_{\text{NaP}}$  would also reduce the slope (gain) of the  $f/I$  relation, which was intuitively quite unexpected. Nevertheless, when we tested these predictions experimentally by using dynamic clamp, the experiments confirmed both the model predictions (see Fig. 11 and Section 5.2, below).

## 5 $I_{\text{NaP}}$ Functions in Hippocampal Pyramidal Neurons

### 5.1 Effects of $I_{\text{NaP}}$ on After-Hyperpolarizations

In most kinds of neurons, single action potentials and spike bursts are followed by AHPs, mainly caused by activation of various voltage- and calcium-gated potassium conductances that outlast the spikes (Vogalis et al., 2003). These AHPs exert feedback regulation of neuronal excitability, shaping the spike pattern through spike frequency adaptation and other effects (Madison & Nicoll, 1984; Storm, 1989, 1990; Pedarzani & Storm, 1993; Peters et al., 2005; Gu et al., 2007). Since  $I_{\text{NaP}}$  is caused by a negative slope resistance that should be capable of amplifying any voltage deflection within its activation range (Crill, 1996; Stuart, 1999; Hu et al., 2002), we expected that  $I_{\text{NaP}}$  would enhance the AHP amplitudes in a voltage-dependent manner, just like it enhances subthreshold resonance and oscillations in these cells (Hu et al., 2002).

To test this idea, we first used our CA1 pyramidal cell model to simulate experiments (Fig. 9) (Vervaeke et al., 2006). Steady current injection (DC) was used to adjust the initial membrane potential to various levels, ranging from  $-58$  to  $-80$  mV, while action potentials were triggered by brief current pulses superimposed on the DC. As expected, the simulations showed that  $I_{\text{NaP}}$  enhanced the AHPs in a voltage-dependent manner in the model (Fig. 9A). In these simulations, we triggered more spikes when injecting a hyperpolarizing DC “holding current” than when using depolarizing DC, in order to be able to compare the impact of  $I_{\text{NaP}}$  on AHPs of similar amplitudes at different potentials, in spite of the voltage-dependent change in  $\text{K}^+$  driving force. However, the spike number was always kept constant with and without  $I_{\text{NaP}}$ , and similar effects were seen also when the spike number was kept constant at different potentials.

To test whether  $I_{\text{NaP}}$  actually has such an amplifying effect also in real CA1 pyramidal cells, we repeated the same protocol during dual whole-cell recordings in rat hippocampal slices (Fig. 1) before and after canceling  $I_{\text{NaP}}$  with the dynamic clamp (Fig. 9B). Again, we used DC to adjust the initial membrane potential. We found that cancellation of  $I_{\text{NaP}}$  reduced the AHPs in a voltage-dependent manner, as predicted theoretically and by the model simulations (Fig. 9A). This implies that  $I_{\text{NaP}}$  amplifies the AHPs, as expected (Vervaeke et al., 2006).

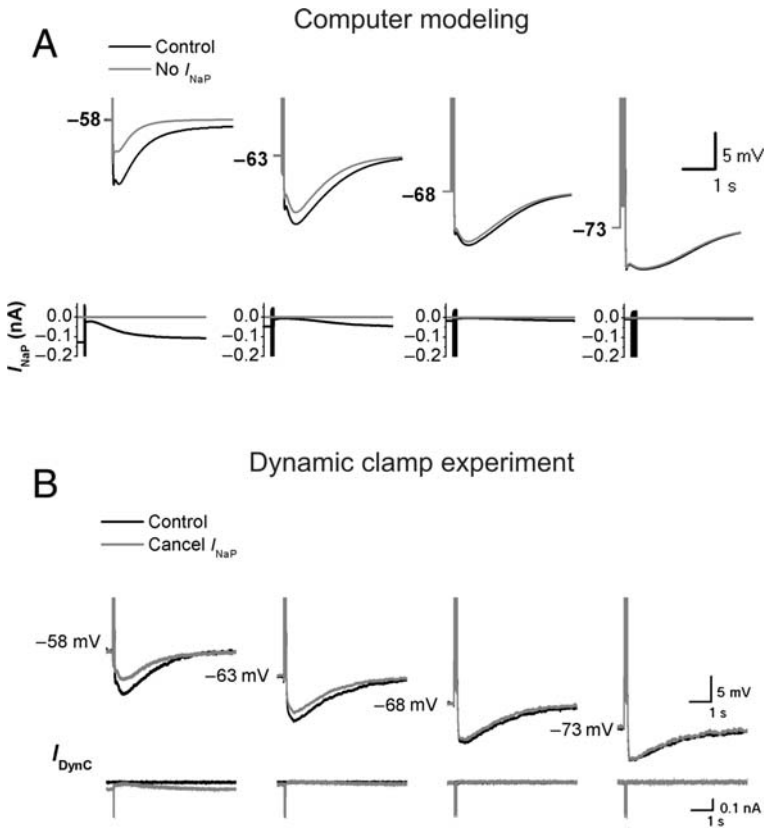


**Fig. 9 Voltage-dependent amplification of after-hyperpolarizations (AHPs) by  $I_{\text{NaP}}$ : comparing computational model predictions with dynamic-clamp experiments. (A) Model simulations of AHPs evoked by spike trains, at different holding potentials (maintained by steady current injection), before (*black*) and after (*gray*) removing  $I_{\text{NaP}}$ . (B) AHPs evoked by action potentials before (*black*) and after (*gray*) canceling  $I_{\text{NaP}}$  by dynamic clamp. In both (A) and (B) each action potential was triggered by a brief, depolarizing current pulse (1–2 ms) and the spike number was adjusted to yield AHPs of similar amplitude for all holding potentials before eliminating  $I_{\text{NaP}}$ . In each case,  $I_{\text{NaP}}$  is plotted below the voltage traces. (Modified from Vervaeke et al., 2006, with permission from *Cell Press, Elsevier*.)**

### 5.2 Effects of $I_{\text{NaP}}$ on Intrinsic Subthreshold Theta Oscillations

Intrinsic, subthreshold membrane potential oscillations can be important determinants of neuronal integration, neuronal coding, and discharge patterns, and can support coherent network oscillations (Llinas, 1988; Singer, 1993; Steriade et al., 1993; Buzsaki, 2006). In the hippocampal formation, slow network oscillations in the theta frequency band (4–10 Hz) are prominent (Vanderwolf, 1988; Buzsaki, 2002). Even when isolated by synaptic blockade, spiny stellate

cells of the EC and hippocampal pyramidal neurons show subthreshold membrane potential oscillations and resonance within the theta frequency band, which are likely to support network theta and neuronal coding within this system (Alonso & Llinas, 1989; Leung & Yu, 1998; Pike et al., 2000; Buzsaki, 2002; Hu et al., 2002). By combining electrophysiology and modeling, we previously found that the subthreshold theta resonance in depolarized CA1 pyramidal cells is due to an interplay between  $I_{\text{NaP}}$  and the  $\text{Kv7/KCNQ/M}$ -type potassium current ( $I_{\text{M}}$ ), while the theta resonance in hyperpolarized cells is due to h/HCN current ( $I_{\text{h}}$ ) (Hu et al., 2002). Although the prominent perithreshold theta resonance and oscillations in depolarized EC stellate cells depend on  $I_{\text{h}}$  rather than  $I_{\text{M}}$ , these theta oscillations also depend on  $I_{\text{NaP}}$  (Alonso & Llinas, 1989). However, in the EC stellate neurons, there is evidence that not only  $I_{\text{NaP}}$  and  $I_{\text{h}}$  are needed for perithreshold oscillations; ion channel noise caused by persistent  $\text{Na}^+$  channels also appears to be essential for these oscillations to appear (Dorval, Jr. & White, 2005).

To further examine the role of  $I_{\text{NaP}}$  in subthreshold membrane potential oscillations of hippocampal CA1 pyramidal neurons, we used dynamic clamp to cancel  $I_{\text{NaP}}$  in hippocampal CA1 pyramidal neurons in hippocampal slices from young rats (4–10 weeks of age) at 30°C (Fig. 10). The methods were identical to those used in our previous study (Vervaeke et al., 2006). In all neurons tested ( $n = 5$ ), we found that cancellation of  $I_{\text{NaP}}$  strongly suppressed the subthreshold theta oscillations (Fig. 10B). The suppression by dynamic clamp was virtually as efficient as blockade of all  $\text{Na}^+$  channels by bath application of 1.0  $\mu\text{M}$  TTX (Fig. 10A). Since TTX blocks the macroscopic  $I_{\text{NaP}}$  as well as the ion channel noise caused by stochastic opening of  $\text{Na}^+$  channels, these result suggest that subthreshold oscillations in CA1 pyramidal neurons depend on  $I_{\text{NaP}}$  as an amplification mechanism, probably in addition to intrinsic channel noise that is needed to trigger the depolarizing waves that constitute these oscillations.

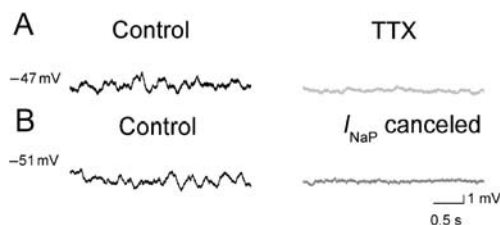


**Fig. 10**  $I_{\text{NaP}}$  is necessary for subthreshold membrane potential oscillations in the theta frequency range in CA1 hippocampal pyramidal neurons. (A) Typical subthreshold membrane potential oscillations before and after blockade of  $I_{\text{NaP}}$  by bath application of 1  $\mu\text{M}$  TTX. (B) Typical subthreshold membrane potential oscillations before and after canceling  $I_{\text{NaP}}$  with dynamic clamp. All traces were recorded at 30°C in the presences of synaptic blockers (10  $\mu\text{M}$  DNQX (6,7-dinitroquinoxaline-2,3-dione) and 10  $\mu\text{M}$  bicuculline free base, which block glutamatergic and GABAergic fast synaptic transmission). (H. Hu et al., unpublished data, 2006.)

### 5.3 Effects of $I_{NaP}$ on Current-to-Frequency Transduction

Many neurons and sensory cells are capable of translating the intensity of a sustained excitatory synaptic barrage, sensory stimuli, or current injection ( $I$ ) into a train of repetitive firing in which the action potential frequency ( $f$ ) encodes the stimulus intensity – the so-called current-to-frequency transduction or frequency coding (Hodgkin, 1948; Kernell, 1965; Connor & Stevens, 1971). This function has been studied in CA1 hippocampal pyramidal cells, like in many other neurons, by injecting a depolarizing current ( $I$ ) into the cell and plotting the spike frequency ( $f$ ) as a function of the current intensity ( $f/I$  plot) (Lanthorn et al., 1984; Madison & Nicoll, 1984). These studies, as well as studies indicating that AHPs are important regulators of the  $f/I$  relation (Kernell, 1965; Madison & Nicoll, 1984; Storm, 1989; Pedarzani & Storm, 1993), suggested that  $I_{NaP}$  is likely to strongly affect the current-to-frequency transduction.

To test these ideas (Vervaeke et al., 2006), we first performed model simulations (Fig. 11A). Surprisingly, these simulations predicted that  $I_{NaP}$  would have two almost opposite or contrasting effects on the excitability of the cell. On one hand, the model predicted that  $I_{NaP}$  would reduce the minimal current necessary to evoke spiking (rheobase), as intuitively expected, because  $I_{NaP}$  naturally will help excite the cell, essentially by adding to the injected current,  $I$ . Thus, as shown in Fig. 11A (left), the base of the simulated  $f/I$  plot was shifted to the right when  $I_{NaP}$  was omitted from the model (gray curve). On the other hand, the model predicted that  $I_{NaP}$  would also reduce the steepness of the  $f/I$  relation (the  $f/I$  slope or gain), as shown by the superimposed  $f/I$  plots to the right in Fig. 11A. This result was surprising, because  $I_{NaP}$ , being an inward current activated by depolarization, might be expected to be activated more, and thus contribute more excitation, the more depolarizing current one injects. Nevertheless, when we tested these predictions experimentally by canceling  $I_{NaP}$  with dynamic clamp, the experiments confirmed both of the two model predictions: the foot of the  $f/I$  curve was shifted to the right, but the curve became steeper (Fig. 11B) (Vervaeke et al., 2006). The effect on the  $f/I$  slope is likely due to a complex interplay between,  $I_{NaP}$ ,  $I_{NaT}$ , AHPs, and other factors.

### 5.4 Effects of $I_{NaP}$ on Firing Regularity

The  $f/I$  experiments also showed that  $I_{NaP}$  strongly affected the regularity of repetitive firing in CA1 pyramidal cells (Fig. 12) (Vervaeke et al., 2006). Thus, canceling of  $I_{NaP}$  by dynamic clamp made the steady-state repetitive firing far less regular (Fig. 12, right), attenuated the peaks in the autocorrelation plots of spike timing (bottom), and significantly increase in the coefficient of variation of the interspike intervals, in all cells tested (data not shown here; Vervaeke et al., 2006).

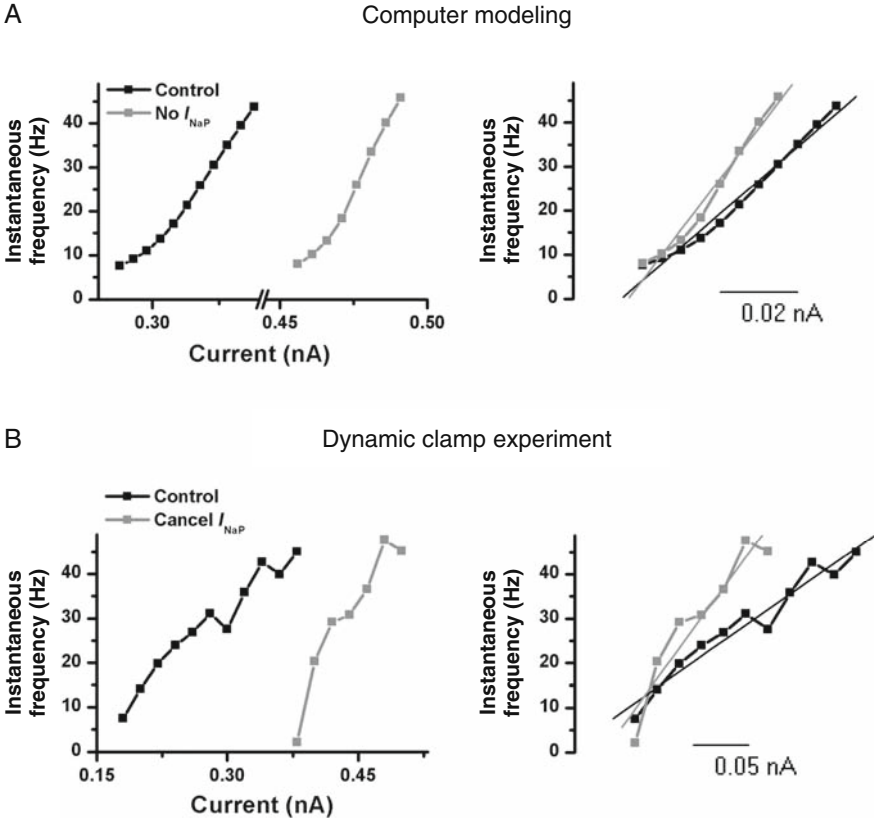


**Fig. 11** Effects of  $I_{NaP}$  on the input–output relation in CA1 pyramidal neurons. Comparing model predictions with dynamic-clamp experiments of current ( $I$ )-to-spike frequency ( $f$ ) transduction. **(A)** Frequency–current ( $f/I$ ) plots with  $I_{NaP}$  (black: control) and without  $I_{NaP}$  (grey) of the average frequency of the first four spikes (range  $\sim 15$ – $60$  Hz) in response to injection of 1-s-long current pulses. The  $f/I$  slope for this range increased by 78 % when  $I_{NaP}$  was blocked, as shown by the fitted linear functions (upper right). **(B)** Experimental  $f/I$  plots obtained from a CA1 pyramidal cell according to the protocol described in (A), before (black) and after (gray) canceling  $I_{NaP}$  by dynamic clamp. Linear fits of the  $f/I$  curves (right panels) showed that canceling  $I_{NaP}$  increased the  $f/I$  slope, on average by 43% for all cells tested ( $n = 7$ ,  $p = 0.015$ ). (Modified from Vervaeke et al., 2006, with permission from *Cell Press, Elsevier*.)

We noted that cancellation of  $I_{NaP}$  caused the expected reduction in AHP amplitude between spikes (Fig. 9), but also a slightly higher spike threshold and lower spike amplitude and rate of rise. These observations suggest that in the absence of  $I_{NaP}$ , the shallower AHPs amplitudes allowed less than normal recovery from inactivation of the spike-generating  $Na^+$  current,  $I_{NaT}$ , during each interspike interval. Under these conditions, the remaining active  $I_{NaT}$  channels may be so few that channel noise becomes more important for spike initiation, thus causing more irregular repetitive firing (Skaugen & Walløe, 1979; Schneidman et al., 1998).

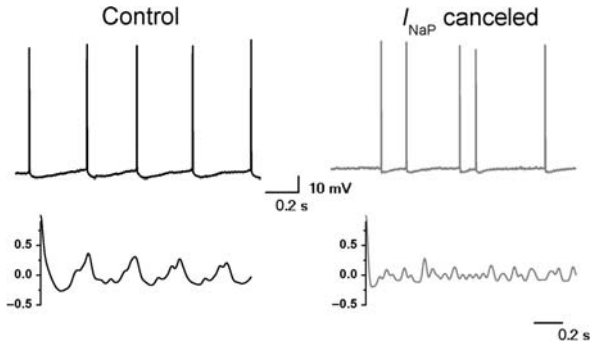


**Fig. 12**  $I_{\text{NaP}}$  maintains regularity of repetitive firing in CA1 pyramidal neurons. (*Left*) Steady-state (fully adapted) repetitive firing of a CA1 pyramidal cell in response to a constant depolarizing current injection under normal conditions (*black trace*). When  $I_{\text{NaP}}$  was canceled by dynamic clamp (*right, gray trace*), the firing became less regular. The intensity of the injected steady current was adjusted to keep a constant average firing rate ( $\sim 3$  Hz) in both conditions. The autocorrelation plots shown below (digitally filtered at 15 Hz) indicate that the regularity of firing was reduced when  $I_{\text{NaP}}$  was canceled ( $n = 6$ ). (Modified from Vervaeke et al., 2006, with permission from *Cell Press, Elsevier*.)

### 5.5 Effects of $I_{\text{NaP}}$ on Spike Timing Precision

We also used dynamic clamp to test how  $I_{\text{NaP}}$  affects the precision of spike timing in response to near-threshold excitatory synaptic input (EPSPs). Holding the CA1 cells at a slightly depolarized potential ( $\sim -60$  mV), we evoked EPSPs by stimulating afferent glutamatergic axons in *stratum radiatum*, at just sufficient intensity to evoke an action potential on about every other EPSP (50% probability). Under normal conditions, spike latency was highly variable (Fig. 13A, left), but this variability was strongly reduced as soon as we canceled  $I_{\text{NaP}}$  by dynamic clamp, readjusting the stimulus strength to achieve once again a 50% spike probability (Fig. 13A, right). Thus, these results support the conclusions of Fricker & Miles (2000) who suggested that  $I_{\text{NaP}}$  reduces spike precision. We also noticed that the subtraction of  $I_{\text{NaP}}$  by dynamic clamp reduced both the rise time and decay time of the EPSPs (Fig. 13B, left), and reduced the plateau potentials or prepotentials from which the spikes often arose in the presence of  $I_{\text{NaP}}$  (Lanthorn et al., 1984; Hu et al., 1992; Fricker & Miles, 2000). Naturally, loss of  $I_{\text{NaP}}$  also reduced the EPSP amplitude, but this was compensated in these experiments by increasing the stimulation intensity, in order to maintain  $\sim 50\%$  firing probability both with and without cancellation of  $I_{\text{NaP}}$ . The sharper peak of the EPSP and the loss of plateau potentials in the absence of  $I_{\text{NaP}}$ , provides less room for random noise-triggered changes in spike latency. This is a likely cause of the increased spike timing precision when the effect of  $I_{\text{NaP}}$  was suppressed (Fig. 13A).

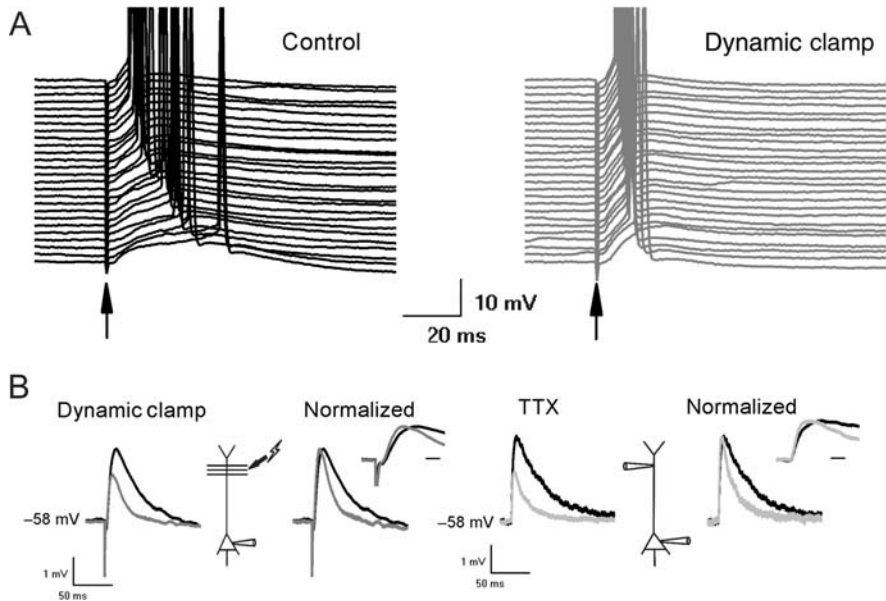


**Fig. 13**  $I_{NaP}$  reduces spike timing precision in response to synaptic input. (A) Somatic recordings of excitatory synaptic potentials (EPSPs) evoked by stimulating dendritic excitatory synapses (axons in the middle of *stratum radiatum*). The EPSPs triggered a spike with a probability of 0.48. When  $I_{NaP}$  was canceled by dynamic clamp, the stimulation strength had to be increased to evoke spikes with a similar probability as before (0.41). (B, left) Subthreshold EPSPs were evoked by stimulating axons in *stratum radiatum* (100  $\mu$ M APV (2- amino-5-phosphonovalerate) was present to block *N*-methyl-d-aspartate (NMDA)-type glutamate receptors). (B, right) A simulated EPSP current waveform was injected through a whole-cell patch pipette on the apical dendrite  $\sim$ 220  $\mu$ m from the soma. Bicuculline free base (10  $\mu$ M) was present throughout all experiments (Modified from Vervaeke et al., 2006, with permission from *Cell Press, Elsevier*.)

In order to compare the effects of dynamic clamp with complete  $Na^+$  channel blockade with TTX, we also performed dual dendritic and somatic whole-cell recordings (Fig. 13B, right). After patching the apical dendrite 180–320  $\mu$ m from the soma, an EPSP-like current waveform was injected into the dendrite to evoke an artificial somatic “EPSP” (aEPSP). Like the dynamic clamp, application of 1  $\mu$ M TTX to the slice reduced both the rise time and decay time of the somatic aEPSP (Fig. 13B, right). These similarities indicate that our somatically applied dynamic “point” clamp was able to efficiently cancel the effects of  $I_{NaP}$  even on EPSPs of distal dendritic origin. Hence, the observed amplifying and slowing effects is entirely or largely due to an  $I_{NaP}$  that originates close to the soma since it is so well controlled by our somatic dynamic clamp. Thus, these results lend further, independent support to our conclusion that  $I_{NaP}$  in CA1 pyramidal cells is probably caused by  $Na^+$  channels concentrated at the axon initial segment, which was part of the justification for using somatic dynamic clamp to study the functional roles of this current in the first place (Fig. 2).

## 6 Concluding Remarks

Based on the experiences described above, we conclude that somatic dynamic clamp is an extremely useful tool for studying the functions of the persistent sodium current,  $I_{\text{NaP}}$ . Although the Na<sup>+</sup> current model that was used in our CA1 hippocampal pyramidal neuron model simulations contained only a simple HH model of  $I_{\text{NaP}}$  combined with a relatively simple four-state Markov model of the transient current,  $I_{\text{NaT}}$ , it successfully predicted and reproduced several key features of the Na<sup>+</sup> current-dependent response properties of the rat CA1 pyramidal cells. Our findings suggest that the main effects of  $I_{\text{NaP}}$  in these cells are quite robust, and therefore may be produced by any fast, persistent inward current with at least roughly the correct voltage dependence combined with a largely perisomatic subcellular distribution.

Considering the advantages of dynamic clamp over pharmacological manipulations for in vivo experiments, the use of this method for studying the functional roles of  $I_{\text{NaP}}$  and other currents in intact and active networks, holds great promise.

**Acknowledgments** Our work was supported by the Norwegian Research Council (NFR) through FUGE, NevroNor, and the Norwegian Centre of Excellence programs, and by HFSP for Research Grant RGP0049 to L.J.G. and J.F.S.

## References

- Aldrich RW, Corey DP, & Stevens CF (1983). A reinterpretation of mammalian sodium channel gating based on single channel recording. *Nature* **306**, 436–441.
- Alonso A & Llinas RR (1989). Subthreshold Na<sup>+</sup>-dependent theta-like rhythmicity in stellate cells of entorhinal cortex layer II. *Nature* **342**, 175–177.
- Alzheimer C, Schwindt PC, & Crill WE (1993). Modal gating of Na<sup>+</sup> channels as a mechanism of persistent Na<sup>+</sup> current in pyramidal neurons from rat and cat sensorimotor cortex. *J Neurosci* **13**, 660–673.
- Andreasen M & Lambert JDC (1999). Somatic amplification of distally generated subthreshold EPSPs in rat hippocampal pyramidal neurones. *J Physiol* **519**, 85–100.
- Armstrong CM (1981). Sodium channels and gating currents. *Physiol Rev* **61**, 644–683.
- Astman N, Gutnick MJ, & Fleidervish IA (1998). Activation of protein kinase C increases neuronal excitability by regulating persistent Na<sup>+</sup> current in mouse neocortical slices. *J Neurophysiol* **80**, 1547–1551.
- Astman N, Gutnick MJ, & Fleidervish IA (2006). Persistent sodium current in layer 5 neocortical neurons is primarily generated in the proximal axon. *J Neurosci* **26**, 3465–3473.
- Attwell D, Cohen I, Eisner D, Ohba M, & Ojeda C (1979). The steady state TTX-sensitive (“window”) sodium current in cardiac Purkinje fibres. *Pflugers Arch* **379**, 137–142.
- Benoit E & Escande D (1993). Fast K channels are more sensitive to riluzole than slow K channels in myelinated nerve fibre. *Pflugers Arch* **422**, 536–538.
- Benoit E & Escande D (1991). Riluzole specifically blocks inactivated Na channels in myelinated nerve fibre. *Pflugers Arch* **419**, 603–609.

- Boiko T, Rasband MN, Levinson SR, Caldwell JH, Mandel G, Trimmer JS, & Matthews G (2001). Compact myelin dictates the differential targeting of two sodium channel isoforms in the same axon. *Neuron* **30**, 91–104.
- Boiko T, Van Wart A, Caldwell JH, Levinson SR, Trimmer JS, & Matthews G (2003). Functional specialization of the axon initial segment by isoform-specific sodium channel targeting. *J Neurosci* **23**, 2306–2313.
- Borg-Graham L (1987). Modelling the somatic electrical behavior of hippocampal pyramidal neuron. Massachusetts Institute of Technology. Ref Type: Thesis/Dissertation
- Borg-Graham L (1999). Interpretations of data and mechanisms for hippocampal pyramidal cell models. In *Cerebral cortex*, eds. Ulinski PS, Jones EG, & Peters A, pp. 19–138. Kluwer Academic/Plenum Publishers, New York.
- Brown DA & Adams PR (1980). Muscarinic suppression of a novel voltage-sensitive K<sup>+</sup> current in a vertebrate neurone. *Nature* **283**, 673–676.
- Buzsaki G (2002). Theta oscillations in the hippocampus. *Neuron* **33**, 325–340.
- Buzsaki G (2006). *Rhythms of the brain* Buzsaki Oxford University Press, Oxford.
- Cantrell AR & Catterall WA (2001). Neuromodulation of Na<sup>+</sup> channels: An unexpected form of cellular plasticity. *Nat Rev Neurosci* **2**, 397–407.
- Chandler WK & Meves H (1966). Incomplete sodium inactivation in internally perfused giant axons from *Loligo forbesi*. *J Physiol* **186**, 121P–122P.
- Chao TI & Alzheimer C (1995). Effects of phenytoin on the persistent Na<sup>+</sup> current of mammalian CNS neurones. *neuroreport* **6**, 1778–1780.
- Connor JA & Stevens CF (1971). Prediction of repetitive firing behaviour from voltage clamp data on an isolated neurone soma. *J Physiol* **213**, 31–53.
- Connors BW, Gutnick MJ, & Prince DA (1982). Electrophysiological properties of neocortical neurons in vitro. *J Neurophysiol* **48**, 1302–1320.
- Critt WE (1996). Persistent sodium current in mammalian central neurons. *Ann Rev Physiol* **58**, 349–362.
- Dorval AD, Jr. & White JA (2005). Channel noise is essential for perithreshold oscillations in entorhinal stellate neurons. *J Neurosci* **25**, 10025–10028.
- Duprat F, Lesage F, Patel AJ, Fink M, Romey G, & Lazdunski M (2000). The neuroprotective agent riluzole activates the two P domain K<sup>+</sup> channels TREK-1 and TRAAK. *Mol Pharmacol* **57**, 906–912.
- Enomoto A, Han JM, Hsiao CF, & Chandler SH (2007). Sodium currents in mesencephalic trigeminal neurons from Nav1.6 null mice. *J Neurophysiol* **98**, 710–719.
- French CR & Gage PW (1985). A threshold sodium current in pyramidal cells in rat hippocampus. *Neurosci Lett* **56**, 289–293.
- French CR, Sah P, Buckett KJ, & Gage PW (1990). A voltage-dependent persistent sodium current in mammalian hippocampal neurons. *J Gen Physiol* **95**, 1139–1157.
- Fricker D & Miles R (2000). EPSP amplification and the precision of spike timing in hippocampal neurons. *Neuron* **28**, 559–569.
- Gilly W & Armstrong CM (1984). Threshold channels—a novel type of sodium channel in squid giant axon. *Nature* **309**, 448–450.
- Goldstein SAN, Bockenbauer D, O’Kelly I, & Zilberberg N (2001). Potassium leak channels and the KCNK family of two-p-domain subunits. *Nat Rev Neurosci* **2**, 175–184.
- Gonzalez-Burgos G & Barrionuevo G (2001). Voltage-gated sodium channels shape subthreshold EPSPs in layer 5 pyramidal neurons from rat prefrontal cortex. *J Neurophysiol* **86**, 1671–1684.
- Gu N, Vervaeke K, & Storm JF (2007). BK potassium channels facilitate high-frequency firing and cause early spike frequency adaptation in rat CA1 hippocampal pyramidal cells. *J Physiol* **580**, 859–882.
- Hodgkin AL (1948). The local electric changes associated with repetitive action in a non-medullated axon. *J Physiol* **107**, 165–181.
- Hodgkin AL & Huxley AF (1952). A quantitative description of membrane current and its application to conduction and excitation in nerve. *J Physiol* **117**, 500–544.

- Hotson JR, Prince DA, & Schwartzkroin PA (1979). Anomalous inward rectification in hippocampal neurons. *J Neurophysiol* **42**, 889–895.
- Hu GY, Hvalby O, Lacaille JC, Piercey B, Ostberg T, & Andersen P (1992). Synaptically triggered action potentials begin as a depolarizing ramp in rat hippocampal neurones in vitro. *J Physiol* **453**, 663–687.
- Hu H, Vervaeke K, & Storm JF (2002). Two forms of electrical resonance at theta frequencies, generated by M-current, h-current and persistent Na<sup>+</sup> current in rat hippocampal pyramidal cells. *J Physiol* **545**, 783–805.
- Huang CS, Song JH, Nagata K, Yeh JZ, & Narahashi T (1997). Effects of the neuroprotective agent riluzole on the high voltage-activated calcium channels of rat dorsal root ganglion neurons. *J Pharmacol Exp Ther* **282**, 1280–1290.
- Jensen MS, Azouz R, & Yaari Y (1996). Spike after-depolarization and burst generation in adult rat hippocampal CA1 pyramidal cells. *J Physiol* **492(Pt 1)**, 199–210.
- Jaub M, Beck H, Siep E, Ruschenschmidt C, Speckmann E-J, Ebert U, Potschka H, Freichel C, Reissmuller E, & Loscher W (2002). Effect of phenytoin on sodium and calcium currents in hippocampal CA1 neurons of phenytoin-resistant kindled rats. *Neuropharmacology* **42**, 107–116.
- Kaplan MR, Cho MH, Ullian EM, Isom LL, Levinson SR, & Barres BA (2001). Differential control of clustering of the sodium channels Nav1.2 and Nav1.6 at developing CNS nodes of ranvier. *Neuron* **30**, 105–119.
- Kernell D (1965). The limits of firing frequency in cat lumbosacral motoneurons possessing different time course of afterhyperpolarization. *Acta Physiol Scand* **65**, 87–100.
- Kole MHP, Ilschner SU, Kampa BM, Williams SR, Ruben PC, & Stuart GJ (2008). Action potential generation requires a high sodium channel density in the axon initial segment. *Nat Neurosci* **11**, 178–186.
- Komai S, Licznerski P, Cetin A, Waters J, Denk W, Brecht M, & Osten P (2006). Postsynaptic excitability is necessary for strengthening of cortical sensory responses during experience-dependent development. *Nat Neurosci* **9**, 1125–1133.
- Kuo CC & Bean BP (1994). Slow binding of phenytoin to inactivated sodium channels in rat hippocampal neurons. *Mol Pharmacol* **46**, 716–725.
- Lanthorn T, Storm J, & Andersen P (1984). Current-to-frequency transduction in CA1 hippocampal pyramidal cells: Slow prepotentials dominate the primary range firing. *Exp Brain Res* **53**, 431–443.
- Leung LS & Yu HW (1998). Theta-frequency resonance in hippocampal CA1 neurons in vitro demonstrated by sinusoidal current injection. *J Neurophysiol* **79**, 1592–1596.
- Lien CC & Jonas P (2003). Kv3 potassium conductance is necessary and kinetically optimized for high-frequency action potential generation in hippocampal interneurons. *J Neurosci* **23**, 2058–2068.
- Lipowsky R, Gillessen T, & Alzheimer C (1996). Dendritic Na<sup>+</sup> channels amplify EPSPs in hippocampal CA1 pyramidal cells. *J Neurophysiol* **76**, 2181–2191.
- Llinas R & Sugimori M (1980). Electrophysiological properties of in vitro Purkinje cell somata in mammalian cerebellar slices. *J Physiol* **305**, 171–195.
- Llinas RR (1988). The intrinsic electrophysiological properties of mammalian neurons: insights into central nervous system function. *Science* **242**, 1654–1664.
- Losonczy A & Magee JC (2006). Integrative properties of radial oblique dendrites in hippocampal CA1 pyramidal neurons. *Neuron* **50**, 291–307.
- Ma M & Koester J (1996). The role of K<sup>+</sup> currents in frequency-dependent spike broadening in alypsia R20 neurons: A dynamic-clamp analysis. *J Neurosci* **16**, 4089–4101.
- Madison DV & Nicoll RA (1984). Control of the repetitive discharge of rat CA 1 pyramidal neurones in vitro. *J Physiol* **354**, 319–331.
- Magee JC & Johnston D (1995). Characterization of single voltage-gated Na<sup>+</sup> and Ca<sup>2+</sup> channels in apical dendrites of rat CA1 pyramidal neurons. *J Physiol* **487(Pt 1)**, 67–90.

- Magistretti J & Alonso A (1999). Biophysical properties and slow voltage-dependent inactivation of a sustained sodium current in entorhinal cortex layer-II principal neurons: A whole-cell and single-channel study. *J Gen Physiol* **114**, 491–509.
- Magistretti J & Alonso A (2002). Fine gating properties of channels responsible for persistent sodium current generation in entorhinal cortex neurons. *J Gen Physiol* **120**, 855–873.
- Mattson RH, Cramer JA, Collins JF, Smith DB, gado-Escueta AV, Browne TR, Williamson PD, Treiman DM, McNamara JO, & McCutchen CB (1985). Comparison of carbamazepine, phenobarbital, phenytoin, and primidone in partial and secondarily generalized tonic-clonic seizures. *N Engl J Med* **313**, 145–151.
- McCormick DA, Huguenard JR (1992). A model of the electrophysiological properties of thalamocortical relay neurons. *J Neurophysiol* **68**, 1384–1400.
- Migliore M, Cook EP, Jaffe DB, Turner DA, & Johnston D (1995). Computer simulations of morphologically reconstructed CA3 hippocampal neurons. *J Neurophysiol* **73**, 1157–1168.
- Patlak J (1991). Molecular kinetics of voltage-dependent Na<sup>+</sup> channels. *Physiol Rev* **71**, 1047–1080.
- Pedarzani P & Storm JF (1993). PKA mediates the effects of monoamine transmitters on the K<sup>+</sup> current underlying the slow spike frequency adaptation in hippocampal neurons. *Neuron* **11**, 1023–1035.
- Peters HC, Hu H, Pongs O, Storm JF, & Isbrandt D (2005). Conditional transgenic suppression of M channels in mouse brain reveals functions in neuronal excitability, resonance and behavior. *Nat Neurosci* **8**, 51–60.
- Pike FG, Goddard RS, Suckling JM, Ganter P, Kasthuri N, & Paulsen O (2000). Distinct frequency preferences of different types of rat hippocampal neurones in response to oscillatory input currents. *J Physiol* **529**, 205–213.
- Pinto RD, Elson RC, Szucs A, Rabinovich MI, Selverston AI, & Abarbanel HDI (2001). Extended dynamic clamp: Controlling up to four neurons using a single desktop computer and interface. *J Neurosci Methods* **108**, 39–48.
- Qu Y, Curtis R, Lawson D, Gilbride K, Ge P, DiStefano PS, Silos-Santiago I, Catterall WA, & Scheuer T (2001). Differential modulation of sodium channel gating and persistent sodium currents by the [beta]1, [beta]2, and [beta]3 subunits. *Mol Cell Neurosci* **18**, 570–580.
- Raman IM & Bean BP (1999). Ionic currents underlying spontaneous action potentials in isolated cerebellar purkinje neurons. *J Neurosci* **19**, 1663–1674.
- Rosenkranz JA & Johnston D (2007). State-dependent modulation of amygdala inputs by dopamine-induced enhancement of sodium currents in layer V entorhinal cortex. *J Neurosci* **27**, 7054–7069.
- Schneidman E, Freedman B, & Segev I (1998). Channel stochasticity may be critical in determining the reliability and precision of spike timing. *Neural Comp* **10**, 1679–1703.
- Schwindt PC & Crill WE (1995). Amplification of synaptic current by persistent sodium conductance in apical dendrite of neocortical neurons. *J Neurophysiol* **74**, 2220–2224.
- Shao LR, Halvorsrud R, Borg-Graham L, & Storm JF (1999). The role of BK-type Ca<sup>2+</sup>-dependent K<sup>+</sup> channels in spike broadening during repetitive firing in rat hippocampal pyramidal cells. *J Physiol* **521 Pt 1**, 135–146.
- Singer W (1993). Synchronization of cortical activity and its putative role in information processing and learning. *Annu Rev Physiol* **55**, 349–374.
- Skaugen E & Walløe L (1979). Firing behaviour in a stochastic nerve membrane model based upon the Hodgkin-Huxley equations. *Acta Physiol Scand* **107**, 343–363.
- Stafstrom CE, Schwindt PC, Chubb MC, & Crill WE (1985). Properties of persistent sodium conductance and calcium conductance of layer V neurons from cat sensorimotor cortex in vitro. *J Neurophysiol* **53**, 153–170.
- Stafstrom CE, Schwindt PC, & Crill WE (1982). Negative slope conductance due to a persistent subthreshold sodium current in cat neocortical neurons in vitro. *Brain Res* **236**, 221–226.

- Steriade M, McCormick DA, & Sejnowski TJ (1993). Thalamocortical oscillations in the sleeping and aroused brain. *Science* **262**, 679–685.
- Storm JF (1989). An after-hyperpolarization of medium duration in rat hippocampal pyramidal cells. *J Physiol* **409**, 171–190.
- Storm JF (1990). Potassium currents in hippocampal pyramidal cells. *Prog Brain Res* **83**, 161–187.
- Stuart G & Sakmann B (1995). Amplification of EPSPs by axosomatic sodium channels in neocortical pyramidal neurons. *Neuron* **15**, 1065–1076.
- Stuart G (1999). Voltage-activated sodium channels amplify inhibition in neocortical pyramidal neurons. *Nat Neurosci* **2**, 144–150.
- Stuart GJ & Sakmann B (1994). Active propagation of somatic action potentials into neocortical pyramidal cell dendrites. *Nature* **367**, 69–72.
- Taddese A & Bean BP (2002). Subthreshold sodium current from rapidly inactivating sodium channels drives spontaneous firing of tuberomammillary neurons. *Neuron* **33**, 587–600.
- Traub RD, Jefferys JG, Miles R, Whittington MA, & Toth K (1994). A branching dendritic model of a rodent CA3 pyramidal neurone. *J Physiol* **481**, 79–95.
- Urban NN, Henze DA, & Barrionuevo G (1998). Amplification of perforant-path EPSPs in CA3 pyramidal cells by LVA calcium and sodium channels. *J Neurophysiol* **80**, 1558–1561.
- Urbani A & Belluzzi O (2000). Riluzole inhibits the persistent sodium current in mammalian CNS neurons. *Eur J Neurosci* **12**, 3567–3574.
- Vandenberg CA & Bezanilla F (1991). A sodium channel gating model based on single channel, macroscopic ionic, and gating currents in the squid giant axon. *Biophys J* **60**, 1511–1533.
- Vanderwolf CH (1988). Synchronization of cortical activity and its putative role in information processing and learning. *Int Rev Neurobiol* **20**, 225–340.
- Vervaeke K, Hu H, Graham LJ, & Storm JF (2006). Contrasting effects of the persistent Na<sup>+</sup> current on neuronal excitability and spike timing. *Neuron* **49**, 257–270.
- Vogalis F, Storm JF, & Lancaster B (2003). SK channels and the varieties of slow after-hyperpolarizations in neurons. *Eur J Neurosci* **18**, 3155–3166.
- White JA, Rubinstein JT, & Kay AR (2000). Channel noise in neurons. *Trends Neurosci* **23**, 131–137.
- Williams SR (2004). Spatial compartmentalization and functional impact of conductance in pyramidal neurons. *Nat Neurosci* **7**, 904–905.
- Yue C, Remy S, Su H, Beck H, & Yaari Y (2005). Proximal persistent Na<sup>+</sup> channels drive spike afterdepolarizations and associated bursting in adult CA1 pyramidal cells. *J Neurosci* **25**, 9704–9720.